Stochastic Models in Geosystems, Eds. S. A. Molchanov, W. A. Woyczynski, IMA Volumes in Mathematics and its Applications, 269 - 312, **85.**

THE MORPHOLOGY AND TEXTURE OF ANISOTROPIC MULTIFRACTALS USING GENERALIZED SCALE INVARIANCE

S. PECKNOLD*, S. LOVEJOY* , AND D. SCHERTZER†

Abstract. Although scale invariance is a basic geodynamic symmetry, there is no reason to expect it to be isotropic; that the corresponding fractals or multifractal fields be self-similar. The analysis of various geophysical fields has indeed shown that although they are typically scaling multifractals, they are indeed anisotropic involving differential rotation, stratification and more complex scale changes. The framework for the analysis and simulation of such fields is generalized scale invariance (GSI), which comprises two elements — the generator and the unit ball. Although the generator is more fundamental, the shape of the possibly highly anisotropic unit ball will also affect the texture and morphology of the corresponding fields. While full nonlinear GSI is difficult to examine, linear approximations are always valid over finite ranges of scale; we will therefore focus on the latter. Building on earlier work using linear GSI and second order (convex/elliptical) balls, we establish a method of constructing higher order families necessary for modeling qualitatively different morphologies, especially non-convex ones. We illustrate the method using fourth order polynomials and multifractal simulations.

1. Introduction. Scale invariant dynamics are generally associated with multifractal fields, and indeed over twenty geophysical fields have been explicitly shown to be multifractal (for a summary and intercomparison, see [Lovejoy and Schertzer, 1995] and [Pecknold et al., 1993]). Since scaling is a statistical symmetry and geophysics deals with fields involving large numbers of degrees of freedom, stochastic geodynamical models provide a natural framework for their study. Indeed, stochastic scaling models have many advantages over the usual deterministic ones, not least because they can be valid over arbitrarily large ranges of scale and thus avoid the ad hoc homogeneity and parametrization assumptions that plague standard approaches based on integrations of (nonlinear) partial differential equations representing the dynamics.

Active fields of research into multifractality in geophysics include turbulence in the temperature [Schmitt et al., 1993] and the wind fields [Meneveau et al., 1990; Schmitt et al., 1992; Schmitt et al., 1993;Chigirinskaya et al., 1994; Lazarev et al., 1994], rainfall and cloud fields [Schertzer and Lovejoy, 1985b; Lovejoy et al., 1987; Gabriel et al., 1988; Gupta and Waymire, 1993; Tessier et al., 1993a], topography [Lovejoy and Schertzer, 1990; Lavallée et al., 1993; Lovejoy et al., 1995], ocean surfaces [Tessier et al., 1993b], sea ice [Falco et al., 1995] and the seismic moment field [Hooge, 1993; Hooge et al., 1994]. These multifractal fields are the generic re-

* Department of Physics, McGill University 3600 University Street, Montreal, Quebec, H3A 2T8, Canada.

† Université Pierre et Marie Curie, Bôite 99, 4 place Jussieu, 75252 Paris Cedex 05, France.

sult of multiplicative cascades and exhibit fractal structures, extreme variability/intermittency (including catastrophic events associated with self-organized criticality; [Schertzer and Lovejoy, 1995b]), as well as other realistic features.

In its simplest form, scale-invariance is self-similar; the resulting multifractals are isotropic exhibiting no preferred direction in space. However, no geophysical field is ever exactly isotropic: for example, due to gravity they are almost invariably stratified in the vertical direction. In addition to the vertical, other preferred directions can arise due to the Coriolis or other forces; sometimes they can even be imposed by external boundary conditions (see [Davis et al., 1992] for an example). The result is stratification, differential rotation and/or other scale and orientation dependent features, which due to the scaling are associated with texture and morphology.

In spite of its obvious importance, the study — both theoretical and empirical — of anisotropic scale invariance is still in its infancy. For example, Generalized Scale Invariance (GSI) which is the general theoretical framework for handling scaling anisotropy — and in fact for defining the very notion of scale in such a system — is quite recent [Lovejoy and Schertzer, 1985; Schertzer and Lovejoy, 1985b; Schertzer and Lovejoy, 1987; Schertzer and Lovejoy, 1989; Schertzer and Lovejoy, 1991b]. The primary exception is the simplest scale dependent anisotropy, "self-affinity", which involves only compressions of structures along coordinate axes. Whereas there exists a rather general framework of anisotropy, the basic ingredient being the Lie algebra of the possibly stochastic generator of the scaling anisotropy, little has been done to explore it. So far, work done on the already rather general problem — involving both differential rotation as well as differential stratification — has been the development of two analysis methods for estimating GSI parameters: the "Monte Carlo rotating ellipse technique, [Lovejoy et al., 1992; Pflug et al., 1992; Pflug et al., 1993] and the scale invariant generator technique," [Lewis et al., 1995], as well as the development of both fractal [Lovejoy and Schertzer, 1985], and multifractal [Pecknold et al., 1993] models incorporating GSI.

Outside of the GSI framework, (with the exception of the special case of self- affinity) there have been only a few attempts to deal with anisotropy. A recent one [Veneziano et al., 1995] uses a discrete scale ratio version of linear GSI. The latter involves scaling only over integer powers of this ratio; not over arbitrary scale ratios, furthermore, it cannot be obviously extended to the nonlinear case. Another proposal is the ad hoc introduction of differing scaling exponents varying as functions of direction. This method of handling scaling anisotropy has been independently proposed by several authors [Fox and Hayes, 1985; Van Zandt et al., 1990; Pilkington and Todoeschuk, 1993]. Although at first sight this is appealing, it turns out to be quite incompatible with scaling - it necessarily involves absolute, rather than relative, notions of scale. Thus any underlying dynamics will be fundamentally dependent, rather than independent, of size. The physical

motivation for GSI is that it must be the nonlinear dynamics of a system that determines the appropriate notion of scale; the latter should not be imposed from without in an ad hoc manner as is usually the case (for example when Euclidean metrics and self-similarity is assumed). Not too surprisingly GSI has some similarities with (general) relativity in which the distribution of mass and energy determine the metric. However, in GSI the (anisotropic) notion of scale is based on equivalence between different fluxes (e.g; buoyancy fluxes and kinetic fluxes [Schertzer and Lovejoy, 1984; Lazarev et al., 1994]) and therefore is based on measure notions rather than metric ones. Indeed, in GSI, the notion of scale is defined primarily by a scale changing group (with generator $\mathbf{G}$), admitting at least one invariant family of balls B_λ generating a measure of size — and therefore of scale ratio λ — usually taken to be the measure/volume of the balls B_λ and respecting an order relation between these balls (i.e. in an ensemble, metric or measure sense large balls contain smaller balls). It may happen that the unit ball B_1 is or can be chosen as isotropic, and the corresponding scale is therefore called a "sphero-scale," but this is not a general rule.

Although in general, the full (non-linear) GSI will be required to completely describe geophysical fields, over a sufficiently small range of scales one may always approximate this by a linearization; "linear GSI" (this is analogous to the flat-space/special relativity approximation). Therefore, in the following, we limit our discussion to linear GSI in which the generator $\mathbf{G}$ is a matrix. Furthermore, we restrict our attention to two dimensions (mostly horizontal cross-sections are discussed here, although the results also apply to vertical and to space-time cross-sections).

Although the generator is the most important element of GSI since it determines the way that basic structures change with scale, nevertheless, the shape of the unit ball (which in general will itself be anisotropic) also has a large effect on the appearance of the field at a given resolution. In previous empirical work on cloud radiances [Pflug et al., 1991], and on simulations [Pecknold et al., 1993], the simplest linear GSI system was studied in which the frontier of the unit ball (and hence all the balls) were circles or ellipses (i.e. defined by a quadratic form). Empirically, this seemed adequate for handling most clouds (see Figures 1.1a and 1.1b for an example); although certain structures such as cyclones were found to poorly represented. Still other systems such as synthetic aperture radar ice fields (see Figures 1.2a and b) have thin, elongated fault/fissure type structures which cannot be obtained using linear GSI with quadratic balls. It is plausible that these features in the ice field correspond to squarish and nonconvex balls (below we use fourth order balls to model this). In any case, it seems clear that it would be advantageous to go beyond elliptical balls. Other possible generalizations (not explored here) include the maintenance of the scalar framework but use of nonlinear (possibly stochastic) generators. Alternatively — recognizing the vector and tensor nature of the dynamics — a vector/tensor "Lie cascade," [Schertzer and Lovejoy, 1995a]

framework could be used. For technical reasons outlined below, the next simplest family of balls of interest here are those defined by a quartic form. Our exploration of these fourth order polynomial balls is significantly more difficult than for the corresponding second order case partially because the parameter space is much larger, but primarily because of the difficulty of choosing balls which define the scale uniquely: imposing the "no crossing" condition. Fourth and higher order polynomials are sufficiently complex that we must develop a fairly general technique in order to handle them. The approach can be summarized as follows: first for simplicity, we limit our study to a subset of fourth order polynomials expressible in terms of combinations of quadratic forms. Using quadratic basis matrices, we then obtain simple expressions for the way the balls change with scale as well as a convenient parametrization which enables their shapes to be readily analyzed. Finally, the crossing condition can be simply expressed.

Once the basic families of balls have been described, we illustrate the typical morphologies and textures by making the corresponding anisotropic multifractal simulations. Although this is necessarily insufficient to describe all possible types of anisotropies that may occur, given that most complex geophysical systems are vector and tensor in nature (rather than being limited to cascades of scalar quantities), we will nevertheless see that many interesting phenomena may be described and modeled in this way.

2. Linear GSI. We will now detail the elements of linear GSI, a special case of nonlinear GSI, the outline and basic results of which were developed in [Schertzer and Lovejoy, 1985b]. The basic ingredient for GSI is the scale changing operator T_λ, which for any given scale ratio $\lambda \geq 1$ reduces balls B_λ of scale ratio λ' (the ratio of the system size to the size of the ball), to balls $B_{\lambda\lambda'}$ of scale ratio $\lambda\lambda'$,

$$T_\lambda B_{\lambda'} = B_{\lambda\lambda'} \tag{2.1}$$

T_λ relates the statistical properties at one scale to another and involves only the scale ratio (there is no characteristic "size"), so that $\underline{x}_{\lambda\lambda'} = T_\lambda \underline{x}_{\lambda'}$, where $\underline{x}_{\lambda\lambda'}$, and $\underline{x}_{\lambda'}$ are vectors on $\partial B_{\lambda\lambda'}$ and $\partial B_{\lambda'}$ (their frontiers), respectively. In general, the family of balls are defined as open subsets of our space that form a basis for the topology of that space [Schertzer and Lovejoy, 1985b]. Here, consider the frontier of the balls (see eq. 2.3), rather than the balls themselves, so that each vector belongs uniquely to one frontier.

To be completely defined, GSI needs more than a scale changing operator; it also requires a definition of the unit scale, i.e. B_1, as well as a definition of how to measure the scale. More precisely, we require:

i) The scale changing operator T_λ which is a one parameter multiplicative group, which we will note: $T_\lambda = \lambda^{\mathbf{G}}$, where $\mathbf{G}$ is the generator of the group[1] In the approximation of linear GSI, $\mathbf{G}$ is an $n \times n$ matrix and

[1] The standard convention of $T_\lambda = \lambda^{-\mathbf{G}}$, due to the physical interpretation of a cascade from large to small scales, assumes a reduction in the size of balls with increasing scale ratio. Given $\underline{x}_\lambda = T_\lambda \underline{x}_1$, it is easy [Schertzer and Lovejoy, 1991b; Pflug et al., 1993] to determine that the corresponding scale changing operator $\widetilde{T}_\lambda$ in Fourier space is the one parameter group admitting the transpose of $\mathbf{G}$ as generator:

$$\underline{x}_\lambda = T_\lambda \underline{x}_1; \underline{k}_\lambda = \widetilde{T}_\lambda \underline{k}_1$$
$$T_\lambda = \lambda^{\mathbf{G}} \Rightarrow \{\widetilde{T}_\lambda = \lambda^{-\widetilde{\mathbf{G}}}; \widetilde{\mathbf{G}} = \mathbf{G}^T\}$$

A reduction in real space thus corresponds to a dilation in Fourier space with the transpose of the generator.

$\underline{x}$ is an n-dimensional vector [Lovejoy and Schertzer, 1985; Schertzer and Lovejoy, 1985a]. When $\mathbf{G}$ is a more general (nonlinear) generator, we must define by differential equations using the fact that $\mathbf{G}$ defines infinitesimal transformations.

ii) The unit ball B_1 corresponding to the unit vectors. The balls are other scales are obtained from it by operating with T_λ. With the group properties of T_λ, for any $\lambda_1\lambda_2 = \lambda$, then

$$\begin{aligned} B_\lambda &= T_{\lambda_2} B_{\lambda_1} = T_{\lambda_2} T_{\lambda_1} B_1 \\ &= T_{\lambda_1} B_{\lambda_2} = T_{\lambda_1} T_{\lambda_2} B_1 \end{aligned} \tag{2.2}$$

If an isotropic ball (i.e., circle or sphere) exists, we call the corresponding scale the "spheroscale." In general, B_1 will be defined by an implicit equation:

$$\begin{aligned} B_1 &= \{\underline{x} : f_1(\underline{x}) < 1\}; \\ \partial B_1 &= \{\underline{x} : f_1(\underline{x}) = 1\} \end{aligned} \tag{2.3}$$

Thus,

$$\begin{aligned} B_\lambda &= \{\underline{x} : f_\lambda(\underline{x}) < 1\}, \\ \forall\, \underline{x} :\ & f_\lambda(\underline{x}) = f_1(T_\lambda^{-1}\underline{x}) \end{aligned} \tag{2.4}$$

iii) An increasing function of λ, here given by f_λ; this assures that the frontiers of the balls do not intersect (section 3.4) and that they uniquely define the scale. In [Schertzer and Lovejoy, 1985b], a somewhat more general framework using open balls was proposed (using a measure of the size of the ball rather than the function f).[2] This implies that

$$\frac{\partial f_\lambda}{\partial \lambda} > 0 \tag{2.5}$$

Note that this positivity requirement is necessary to ensure that T_λ corresponds to a scale reduction. Given 2D linear GSI, we may decompose

[2] The use of open balls has the advantage that they generate a topology of our space; in addition, the definition of convex balls, which will be useful to us, is based upon the convexity of their non-empty interior.

G into pseudo-quaternion elements [Lovejoy and Schertzer, 1985; Schertzer and Lovejoy, 1985b; Pecknold et al., 1993; Pflug et al., 1993]:

$$\mathbf{G} = d\mathbf{1} + e\mathbf{I} + f\mathbf{J} + c\mathbf{K} , \tag{2.6}$$

where

$$\mathbf{1} = \begin{pmatrix} 1 & 0 \\ 0 & 1 \end{pmatrix} \quad \mathbf{I} = \begin{pmatrix} 0 & -1 \\ 1 & 0 \end{pmatrix}$$
$$\mathbf{J} = \begin{pmatrix} 0 & 1 \\ 1 & 0 \end{pmatrix} \quad \mathbf{K} = \begin{pmatrix} 1 & 0 \\ 0 & -1 \end{pmatrix}$$

A useful parameter for the description of the overall type of anisotropy present in the system will be given by

$$a^2 = c^2 + f^2 - e^2 \tag{2.7}$$

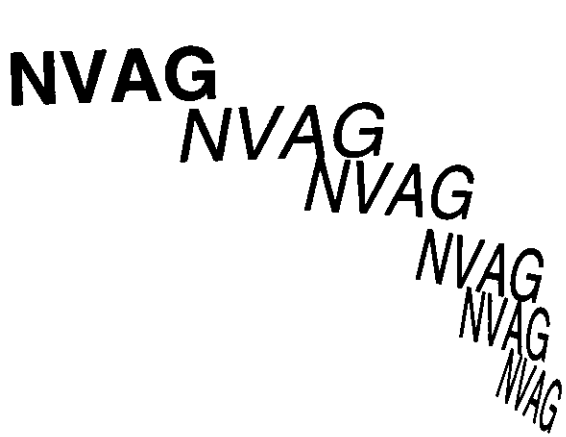

The symbol NVAG is operated upon with an anisotropic scale changing operator, and the result is shown for various scales.

In the case that $a^2 < 0$, we say that the system is rotation dominant; as the scale changes, the balls pass through an infinite degree of rotation (although for a finite total scale ratio, only a finite amount of rotation is possible). If $a^2 > 0$, we call the system stratification dominant; in a like

manner, an indefinitely large "stretching" of the unit ball is permitted, with only a limited amount of rotation. The effect of operating on the vectors of a field with the T_λ operator is demonstrated in the figure above. The effect of the parameters chosen ($c = 0.3, f = -0.5, e = 0.8$) is to rotate and compress the word "NVAG" as the scale to which the vector corresponds is reduced. An isotropic scale changing operator would uniformly shrink the word, with the copies converging toward the center of the reduction.

Thus, we are able to describe the type of linear scaling anisotropy present in a 2D system by determining the values of the parameters describing $\mathbf{G}$. We are able to reduce these four parameters to three, since the value of the parameter d may be renormalized by a different choice of measurement of scale (i.e. a different function f). Since, for example, we do not expect any overall stratification in horizontal cross-sections of the atmosphere: we may take $d = 1$, implying that scale is proportional to the square root of the area of the corresponding balls. In other cases, such as for example the vertical direction of the atmosphere compared to the horizontal direction, there is an overall stratification. In these cases it is more convenient to use the horizontal dimensions to define distance, and we obtain a nontrivial *elliptical* dimension, d_{el} : $d_{el} = Tr(\mathbf{G})$. Thus the parameter d is half of the elliptical dimension. In the case of three-dimensional atmospheric dynamics, this quantity has been estimated to be $d_{el} = 23/9 (= 2.555)$ [Schertzer and Lovejoy, 1985a; Chigirinskaya et al., 1994; Lazarev et al., 1994]. Similarly, in (x, y, z, t) space, rain has been estimated to have $d_{el} = 2.89$ [Lovejoy et al., 1987; Tessier et al., 1993a]. In our case, where we expect no overall stratification, $d_{el} = 2$.

3. Polynomial balls.

3.1. Discussion. In linear GSI, T_λ is simply a linear transformation; we seek a simply connected family of balls which is invariant under linear coordinate transformations, i.e. polynomials. In order to simplify both the analysis and simulation of fields in view of the extensive use of Fourier techniques, we consider even order polynomials with the additional invariance under inversion, $\underline{x} \to -\underline{x}$. The simplest examples are the quadratic forms, characterized by the equation

$$f_1(\underline{x}) = \underline{x}^T \mathbf{A}_1 \underline{x} = 1 \tag{3.1}$$
$$\mathbf{A}_1 = \begin{pmatrix} A_{00} & A_{01} \\ A_{01} & A_{11} \end{pmatrix}$$

where $\underline{x} = (x, y)$ is a positive vector on the frontier of the unit ball, and $\mathbf{A}_1$ is a symmetric 2×2 matrix describing the unit ball. The lack of a subscript on the position vectors will henceforth be taken to mean vectors on the frontier of the unit ball unless otherwise specified.

Only ellipses have been discussed since hyperbolae and parabolae do

not form closed curves.[3] Hence, we have the constraints $A_{00}, A_{11} > 0$ and $A_{00}A_{11} - A_{01}^2 > 0$. This equation thus describes an ellipse or circle. According to eq. 2.1 a generalized magnification by factor λ of any vector $\underline{x}_1$ of the frontier of the unit ball B_1 satisfies:

$$\underline{x}_\lambda = T_\lambda \underline{x}_1 = \lambda^{-\mathbf{G}} \underline{x}_1 \tag{3.2}$$

Defining $f_\lambda(\underline{x}) = \underline{x}^T \mathbf{A}_\lambda \underline{x}$, we have:

$$\mathbf{A}_\lambda = (T_\lambda^{-1})^T \mathbf{A}_1 T_\lambda^{-1} = \lambda^{-\mathbf{G}^T} \mathbf{A}_1 \lambda^{-\mathbf{G}} \tag{3.3}$$

The case in both linear and nonlinear GSI was discussed extensively in [Schertzer and Lovejoy, 1985b]; see section 3.4.

3.2. A basis of scaling symmetric matrices. To understand the transformation of these matrices, it is convenient (although not indispensable) to decompose $\mathbf{A}_1$ into symmetric (quadratic) basis matrices $\mathbf{m}_1, \mathbf{m}_2, \mathbf{m}_3$

$$\mathbf{A}_1 = \sum_{i=1}^{3} \alpha_{i,1} \mathbf{m}_i \tag{3.4}$$

These 3 basis symmetric matrices are defined by being scaling for the T_λ transformation:

$$\lambda^{\mathbf{G}^T} \mathbf{m}_i \lambda^{\mathbf{G}} = \lambda^{\wedge_i} \mathbf{m}_i \tag{3.5a}$$

Hence the differential action of T_λ on $\mathbf{A}$ corresponding to the integral one given by eq. 3.2 is $\lambda \frac{dA_\lambda}{d\lambda} = sym(A_\lambda G)$, this scaling property corresponds to an eigenvalue problem:

$$\wedge_i \mathbf{m}_i = \mathbf{G}^T \mathbf{m}_i + \mathbf{m}_i \mathbf{G} = sym(\mathbf{m}_i \mathbf{G}) = \mathbf{m}_i' \tag{3.5b}$$

with

$$\wedge_1 = 2d, \quad \wedge_2 = 2d - 2a, \quad \wedge_3 = 2d + 2a$$

On this basis, we have corresponding to eq. 3.4, $\mathbf{A}' = \mathrm{sym}(\mathbf{AG}) = \sum_i \alpha_i' \mathbf{m}_i$, with $\alpha_i' = \wedge_i \alpha_i$.

Expressing the $\mathbf{m}_i$ using the pseudoquaternion representation for $\mathbf{G}$ (see eq. 2.3 above) yields the following:

$$\mathbf{m}_1 = \begin{pmatrix} e+f & -c \\ -c & e-f \end{pmatrix} \quad \mathbf{m}_2 = \begin{pmatrix} (e+f)^2 & -(e+f)(c+a) \\ -(e+f)(c+a) & (c+a)^2 \end{pmatrix}$$

$$\mathbf{m}_3 = \begin{pmatrix} (e+f)^2 & -(e+f)(c-a) \\ -(e+f)(c-a) & (c-a)^2 \end{pmatrix} \tag{3.6}$$

[3] The latter can still have a well-defined interior and may ultimately find some application.

With these matrices[4], $\mathbf{A}_\lambda$ are then just given by:

$$\mathbf{A}_\lambda = \lambda^{\mathbf{G}^T} \mathbf{A}_1 \lambda^{\mathbf{G}} = \sum_i \alpha_{i,\lambda} \mathbf{m}_i \tag{3.7}$$
$$\alpha_{i,\lambda} = \alpha_i \lambda^{\wedge_i}$$

For simplicity of notation, in what follows the second (scale ratio) subscript on the parameters $\alpha_1, \alpha_2, \alpha_3$ will be suppressed for the case of the unit matrix $\mathbf{A}_1$.

Of course when $a^2 < 0$, a is imaginary and the above representation for $\mathbf{m}_2, \mathbf{m}_3$ will no longer be useful since it will be complex. In order to deal with this rotation dominance case, note that $\mathbf{m}_2, \mathbf{m}_3$ are complex conjugates (as are Λ_2, Λ_3), and introduce new basis matrices $(\mathbf{m}_4, \mathbf{m}_5)$ which are respectively the real and imaginary parts of $\mathbf{m}_2$:

$$\mathbf{m}_4 = \begin{pmatrix} (e+f)^2 & -(e+f)c \\ -(e+f)c & c^2 - |a|^2 \end{pmatrix} \quad \mathbf{m}_5 = \begin{pmatrix} 0 & -(e+f)|a| \\ -(e+f)|a| & 2c|a| \end{pmatrix} \tag{3.8}$$

and correspondingly

$$\begin{pmatrix} \alpha_{4,\lambda} \\ \alpha_{5,\lambda} \end{pmatrix} = \lambda^{-2d} \begin{pmatrix} \cos 2|a|u & \sin 2|a|u \\ -\sin 2|a|u & \cos 2|a|u \end{pmatrix} \begin{pmatrix} \alpha_4 \\ \alpha_5 \end{pmatrix}$$

where $u = \log \lambda$, and the scale ratio subscript is again suppressed here and henceforth on the unit scale parameters. Note that in this basis,

$$\alpha_4' = 2d\alpha_4 + 2|a|\alpha_5$$
$$\alpha_5' = -2|a|\alpha_4 + 2d\alpha_5$$

Since we will require both the scale changing properties of $\mathbf{A}$ and $\mathbf{A}'$, this quadratic basis is very convenient.

3.3. Elliptical coordinates. In order to understand the action of T_λ on the polynomial balls, it is now useful to perform a change of variables $(x, y) \to (r', \phi)$. Details are to be found in Appendix A. The change into the resulting elliptical coordinates gives the following simplifications for the second order polynomials. In the case of stratification dominance, $a^2 > 0$, we obtain:

$$r'^2 \sin 2\phi = \underline{x}^T \mathbf{m}_1 \underline{x}$$
$$r'^2 (1 - \cos 2\phi) = \underline{x}^T \mathbf{m}_2 \underline{x} \tag{3.9}$$
$$r'^2 (1 - \cos 2\phi) = \underline{x}^T \mathbf{m}_3 \underline{x}$$

[4] The eigenvalue type problem (eq. 3.5b) has unique eigenvalues but not unique eigenvectors, so that the $\mathbf{m}_i$ are not unique. An equally good set is $\mathbf{s}_u \propto (\mathbf{G} - (d - \mu)\mathbf{1})^T (\mathbf{G} - (d - \mu)\mathbf{1}), \mu = \pm a; \mathbf{s}_\mu \propto (\mathbf{G} - d)^T \mathbf{I}, \mu = 0$.

Where r' is the "elliptical radius" (the curve $r' =$ constant is an ellipse), ϕ the polar elliptical angle. The corresponding quadratic forms are thus given by

$$\underline{x}^T \mathbf{A}_\lambda \underline{x} = r'^2(\alpha_{2,\lambda} + \alpha_{3,\lambda} + (\alpha_{2,\lambda} - \alpha_{3,\lambda})\cos 2\phi + \alpha_{1,\lambda} \sin 2\phi) \tag{3.10}$$

while for the case of rotation dominance a different elliptical coordinate system is used, yielding:

$$\begin{aligned} r'^2 &= \underline{x}^T \mathbf{m}_1 \underline{x} \\ r'^2 \cos 2\phi &= \underline{x}^T \mathbf{m}_4 \underline{x} \\ r'^2 \sin 2\phi &= \underline{x}^T \mathbf{m}_5 \underline{x} \end{aligned} \tag{3.11}$$

and the corresponding quadratic form:

$$\underline{x}^T \mathbf{A}_\lambda \underline{x} = r'^2(\alpha_{1,\lambda} + \alpha_{4,\lambda} \cos 2\phi + \alpha_{5,\lambda} \sin 2\phi) \tag{3.12}$$

Since the coefficients $\alpha_{i,\lambda}$ transform trivially with scale, this representation is convenient: the above clearly describes a sinusoidal variation of the contour around the basic ellipse given by $r' =$ constant. Higher order polynomials obtained by using these quadratic forms as building blocks will also be straightforward to express, involving higher order (Fourier) terms in ϕ.

3.4. The non-intersection condition. Every vector over which the field is defined must be associated with only one scale, that is, it must have only one size. A further set of constraints is thus placed on the GSI and unit ball parameters, by the requirement that the balls do not intersect at different scales (i.e. that equation 2.5 holds and the notion of "scale" is uniquely defined. In determining the constraints imposed by this non-crossing condition, it is only necessary to show non-intersection at a given scale. Thus, if we consider the balls defined by

$$\partial B_\lambda = \{\underline{x} : \ f_\lambda(\underline{x}) = 1\} \tag{3.13}$$

with, similarly to eq. 3.1,

$$f_\lambda(\underline{x}) = \underline{x}^T \mathbf{A}_\lambda \underline{x} \tag{3.14}$$

Then the condition that there be no crossing is simply that

$$\frac{\partial f_\lambda(x)}{\partial \lambda} \propto \underline{x}^T \mathbf{A}'_\lambda \underline{x} > 0 \tag{3.15}$$

In this case the non-crossing condition is straightforward; a spectral (eigenvalue) approach shows that it suffices that the real part of the eigenvalues of $\mathbf{A}' = \mathrm{sym}(\mathbf{AG})$ be positive [Schertzer and Lovejoy, 1985b]. Furthermore, since $\underline{x}^T \mathbf{A}'_\lambda \underline{x} = (\lambda^{\mathbf{G}} \underline{x})^T \mathbf{A}_1 (\lambda^{\mathbf{G}} \underline{x})$, if the condition holds at one scale it will

hold any other. It is instructive however to derive this result using the quadratic basis matrices in elliptical coordinates; from (3.9) and (3.11), we find by inspection that the above condition for non-crossing corresponds to:

$$\begin{aligned} &\frac{\alpha_1^2}{\alpha_2 \alpha_3} < 4\left(1 - \frac{a^2}{d^2}\right); \qquad \alpha_2(d-a) + \alpha_3(d+a) > 0; \quad a^2 > 0 \\ &\frac{\alpha_1^2}{\alpha_4^2 + \alpha_5^2} > \left(1 + \frac{|a|^2}{d^2}\right); \qquad \alpha_1 > 0 \qquad\qquad a^2 < 0 \end{aligned} \tag{3.16}$$

which involves both the GSI parameters and the values of α_i. Note that the critical non-crossing conditions here are indeed scale-invariant; hence, if there is no crossing at a given scale, there will be no crossing at any other scale.

We may simplify in the case where a spheroscale exists. A positive spectrum of sym $(\mathbf{AG})$ in the pseudo-quaternion representation with:

$$\mathbf{A} = \delta \mathbf{1} + \varphi \mathbf{J} + \gamma \mathbf{K} \tag{3.17}$$

$$sym(\mathbf{AG}) = D\mathbf{1} + F\mathbf{J} + C\mathbf{K}$$

is obtained if $D > 0$, $D^2 > C^2 + F^2$ where:

$$\begin{aligned} D &= \varphi f + \gamma c + \delta d \\ F &= \delta f - \gamma e + \varphi d \\ C &= \varphi e + \delta c + \gamma d \end{aligned} \tag{3.18}$$

If a scale exists at which $\mathbf{A} = 1$ we obtain a circle; this scale is the spheroscale, and when it exists the restriction is only on the GSI parameters:

$$d > 0; \ d^2 > c^2 + f^2 \tag{3.19}$$

4. Simulations.

4.1. Universal multifractals. We will be interested in simulations of anisotropic multifractals defined by fourth order polynomial balls. Although here we are applying the preceding discussion to the simulation of multifractals, it is equally applicable to monofractals (e.g. generalizations of Brownian motion). We will be particularly interested in the "universal' multifractals. These are the stable, attractive result of nonlinear mixing/interacting multifractal processes. These multifractal fields ε_λ have generators $\log \varepsilon_\lambda$ which are Lévy noises with parameter α. The scaling of the statistical moments of the field, i.e. their dependence upon the scale ratio λ, is determined by the $K(q)$ function, defined as:

$$\lambda^{K(q)} = \langle \varepsilon_\lambda^q \rangle \tag{4.1}$$

where the brackets indicate statistical averaging. In the case of universal multifractals, the (scale-independent) $K(q)$ function is given by:

$$K(q) = \frac{C_1}{\alpha - 1}(q^\alpha - q) \tag{4.2}$$

given that $\alpha \neq 1$, where $0 < \alpha \leq 2$. C_1 is the codimension of the mean of the field, characterizing the sparseness of the mean, and the Lévy index α characterizes the degree of multifractality [Schertzer and Lovejoy, 1987]. As $\alpha \to 0$, $K(q)$, becomes linear and we obtain the monofractal β-model [Novikov and Stewart, 1964; Yaglom, 1966; Mandelbrot, 1974; Frisch et al., 1978]; $\alpha = 2$ corresponds to the "lognormal model (with a Gaussian generator).

For nonconservative fields [Schertzer and Lovejoy, 1987; Schertzer and Lovejoy, 1991a], such as density fields ρ related to a conservative multifractal field ε_λ in a scaling manner ($|\Delta\rho_\lambda| = \varepsilon_\lambda \lambda^{-H}$), there is a third fundamental parameter, H, which is a measure of the degree of (scale by scale) non-conservation of the field:

$$\langle |\Delta\rho_\lambda| \rangle = \lambda^{-H} \tag{4.3}$$

The value of H can be determined from the scaling of the power spectrum and the moment scaling function. $H = 0$ for conservative multifractals which are the direct outcome of multiplicative cascade processes. In general H is the degree of (fractional) integration required to obtain the observed field from the conservative field; for example if ε is the cube root of the energy flux in turbulence and ρ the velocity field, then $H = 1/3$.

5. Fourth-order polynomials.

5.1. Discussion. We now wish to extend our discussion of quadratic balls to higher order polynomial balls, with the particular intent of generating non-convex and non-elliptical shapes which are impossible with quadratic balls. Taking the fourth order case as our example, the general form of our fourth order polynomials involves eight parameters (the coefficients of $x^4, y^4, x^2y^2, x^3y,\ y^3x, x^2, y^2, xy$). Our goal is not to study the most general case; this is unnecessarily complex. It is involves solutions to general quartic equations which are difficult to deal with, and in any case will not always yield closed curves. Rather, we seek a subset of the fourth-order polynomials which is broad enough to display the qualitative features of interest while simultaneously remaining easy to handle empirically and theoretically. It is convenient to consider the family defined by

$$f_1(\underline{x}) = (\underline{x}^T \mathbf{A}_1 \underline{x})^2 + (\underline{x}^T \mathbf{B}_1 \underline{x})^2 = 1 \tag{5.1}$$

where $\mathbf{A}_1, \mathbf{B}_1$ are symmetric 2×2 matrices, and the subscript on the vector $\underline{x}$ is again suppressed as it is on the unit ball. This is a closed family under the GSI transformation which has the additional advantage that the

basic characteristic shapes can be understood from the relation of $\mathbf{A}_1, \mathbf{B}_1$ to the usual quadratic forms (e.g. if det $\mathbf{A}_1 > 0$, we have an ellipse, det $\mathbf{A}_1 < 0$, a hyperbola etc.). This gives a six-parameter family of curves, with parameters $\alpha_1, \alpha_2, \alpha_3, \beta_1, \beta_2, \beta_3$ (or $\alpha_1, \alpha_4, \alpha_5, \beta_1, \beta_4, \beta_5$ for rotation dominant cases), satisfying the previous relations (3.2)–(3.10). The α parameters are defined by eq. (3.4) and depend on the $\mathbf{A}_1$ matrix, while the β parameters are analogous to these for the $\mathbf{B}_1$ matrix. We note that the previously considered family of quadratic balls is included in this family as a subset, with either α_i or β_i being all zero (the only new effect of the additional solutions for the square in this case would be to render the quadratic hyperbolic cases closed; these cases are not very interesting, however, since — except in the trivial case of isotropic reductions — they necessarily cross. The remaining elliptical shapes are identical to those in the previously considered quadratic case.) It remains to be seen which of these have $\partial f_\lambda / \partial \lambda > 0$, i.e. have uniquely defined scales and correspond to reductions when operated on by T_λ. Applying condition 2.5 to the function f defined in eq. 5.1, we obtain the following condition:

$$\frac{\partial f_\lambda(\underline{x})}{\partial \lambda} \propto (\underline{x}^T \mathbf{A}_\lambda \underline{x})(\underline{x}^T \mathbf{A}'_\lambda \underline{x}) + (\underline{x}^T \mathbf{B}_\lambda \underline{x})(\underline{x}^T \mathbf{B}'_\lambda \underline{x}) > 0 \tag{5.2}$$

One way to proceed would be to directly extend the results of the quadratic case; i.e. to require that each factor in the sum above is always positive. We note that for $d > 0$, $d^2 > a^2$, (or equivalently, if $\mathrm{Re}[\sigma(\mathbf{G})] > 0$, where $\sigma(\mathbf{G})$ is the spectrum of $\mathbf{G}$),and if $\underline{x}^T \mathbf{A}' \underline{x} > 0\ \forall\ \underline{x}$, then $\underline{x}^T \mathbf{A} \underline{x} > 0\ \forall\ \underline{x}$. We can thus extend the quadratic case using a direct spectral approach (i.e. considering the sign of the eigenvalues of sym($\mathbf{AG}$) and sym($\mathbf{BG}$)). The benefit of this spectral approach is that it is valid in any dimension of space, not requiring special basis matrices. In this case, though, since positivity of each term is somewhat unnecessarily restrictive (it is a sufficient but not necessary condition), this will lead only to a subset of noncrossing balls, in fact generally different from the ones found below. Since it involves general quartic equations, it does not yield a simple criterion for describing the shapes of the balls, as discussed in section 5.4. Alternatively, the spectral approach can in principle be extended for non-positive spectra of $\mathbf{A}$ and $\mathbf{B}$, or more generally it could be based on quartics defined by fourth rank tensors (rather than the second rank tensors used here); this will be developed in a subsequent paper. In order to obtain a manageable family of non-convex balls, we therefore use a different approach by considering sub-classes (corresponding to subgroups of the transformation of f) easily obtained from the quadratic basis matrices. These sub-classes can be readily obtained by setting the various α's and β's $= 0$. Noting that the cases where $\mathbf{A} = 0$, or $\mathbf{B} = 0$, or all α's but one, all β's but one $= 0$ reduce to convex quadratic balls, we consider four parameter cases with $\alpha_1 = \beta_1 = 0$[5]. All other four-

[5] In terms of determinants the case $a^2 < 0$, $\alpha_1 = \beta_1 = 0$ corresponds to det $\mathbf{A} <$

parameter cases either cross or lead to no appreciable simplification with respect to the full six parameter problem. We note that the four-parameter space for defining unit balls involves only three-parameter families of balls, since any unit ball enlarged by T_λ can be taken as a unit ball. A specific family of balls can now conveniently be represented by defining vectors $\underline{r}_2 = (\alpha_2, \beta_2), \underline{r}_3 = (\alpha_3, \beta_3), (\underline{r}_4 = (\alpha_4, \beta_4), \underline{r}_5 = (\alpha_5, \beta_5)$ in the rotation dominant case). We now define θ to be the angle between the vectors, r the ratio of their magnitudes, and $R^2 = \sqrt{(\alpha_{2,1}^2 + \beta_{2,1}^2)(\alpha_{3,1}^2 + \beta_{3,1}^2)}$ for the stratification dominant case and $R^2 = r_{4,1}^2 + r_{5,1}^2$ for the rotation dominant case as scale invariant measures of magnitude of the vectors (see appendix A).

For stratification dominance, as we change scales, r is proportional to λ^{-4a}, and θ is constant, hence the vectors $\underline{r}_2, \underline{r}_3$ are simply isotropically reduced. In polar (r, θ) space the system evolves along a ray. Furthermore, using the elliptical coordinates, as we change scales, the necessary and sufficient no-crossing conditions are simply that[6]

$$\begin{array}{l} d \geq a \\ \cos\theta \geq 0 \end{array} \tag{5.3}$$

For rotation dominance, we find that the expression:

$$\frac{\sin\theta}{r + r^{-1}}$$

is scale invariant. If we again take (r, θ) as polar coordinates, then the constancy of the above expression defines a circle which is traced out as the system is reduced. Furthermore, necessary and sufficient conditions such that $\partial f_\lambda / \partial \lambda > 0$ (no crossing occurs) are that the vectors $\underline{r}_4$ and $\underline{r}_5$ must be chosen such that:

$$d \geq |a|$$

$$\frac{\sin\theta}{r + r^{-1}} \geq \frac{|a|}{2\sqrt{d^2 + |a|^2}} \tag{5.4}$$

If we take an initial vector ($\underline{r}_4$ say) as a unit vector lying in the x direction, then the allowed (noncrossing) vectors $\underline{r}_5$ will lie within a circle radius $d/|a|$ centred on the y axis at a distance $\sqrt{1 + (d/|a|)^2}$ from the origin. These conditions are scale invariant: it is necessary and sufficient that it be respected at an arbitrary scale. Examples of various possible balls are given in Figures 2 and 3. Note that the requirement that $d \geq |a|$ in both cases effectively restricts us to generators not very far from the identity; however empirical estimates of $|a|$ in various geophysical fields (clouds, topography, ice) show that this does not seem to be a serious practical restriction.

0, $\det \mathbf{B} < 0$ i.e. this family is disjoint to the corresponding one obtained by the above (spectral) sufficiency condition.

[6] Note that for $\alpha_1 = \beta_1$, this condition is equivalent to $\det \mathbf{A} + \det \mathbf{B} > 0$.

Now that we have found noncrossing quartics, it is useful to write them in more familiar form. To start with, note that in the pseudo-quaternion representation (eq. 3.17) the condition $\alpha_1 = 0$ implies (for any value of a^2) that:

$$e\delta = f\gamma - c\varphi \tag{5.5}$$

It is not too hard to show that the condition $\alpha_1 = 0$ remains valid under any linear coordinate transformation. Hence for $a^2 > 0$, any matrices $\mathbf{A}, \mathbf{B}$ which satisfy $\alpha_1 = 0, \beta_1 = 0$ can be put in the form:

$$f = Lu^4 + Mu^2\nu^2 + N\nu^4 \tag{5.6}$$

with

$$\begin{array}{l} u = r' \sin 2\phi \\ \nu = r' \cos 2\phi \end{array} \tag{5.7}$$

Using the above conditions on the α's and β's we require $L > 0$, $N > 0$, and $\sqrt{LN} \geq M > 0$, then no crossing occurs and $\partial f / \partial \lambda > 0$.

A similar expression of the rotation dominant case ($a^2 < 0$) may be obtained; in this case we have

$$f = P(u^4 + \nu^4) + Qu\nu(\nu^2 - u^2) + Ru^2\nu^2 \tag{5.8}$$

with the no crossing conditions becoming $P > 0$, $R > 0$, $4P(R+2P) > Q^2$ and:

$$\frac{\sqrt{4P(R+2P) - Q^2}}{R + 2P} \geq \frac{|a|}{2\sqrt{d^2 + |a|^2}} \tag{5.9}$$

5.2. Stratification dominant examples. Figure 2 shows a series of stratification dominant balls for varying GSI parameters and unit-ball parameters. Figure 4 shows the corresponding real fields. In all these cases, as well as in the examples described below, the fields are simulated using the techniques described in Pecknold et al. (1993), with $\alpha = 1.7, C_1 = 0.1$, and $H = 0.5$. These parameters correspond to those determined for landscape topography [Lavallée et al., 1993], and were chosen primarily for ease of visualization — the codimension of the mean, C_1, is low, thus the mean field is not too sparse, and a moderate degree of smoothing is given by the value of H chosen. The GSI parameters chosen for the stratification dominant examples all gave similar values for a^2, (about 0.4), and display fields where the c parameter dominates, where the f parameter dominates, and where c, f, and e are similar. We note that "typical" values found in

loud data are of about this size [Pflug et al., 1993], as the parameters c nd f are generally limited as in equation (2.7), and the e parameter is ypically also less than 1.

The equation for our balls in the stratification dominant case where $_1 = \beta_1 = 0$ is given by:

$$r'^{-4}(\phi) = \lambda^{-4d} R^2 \left(\frac{3}{2}\left(r + \frac{1}{r}\right) + \cos\theta + 2\left(\frac{1}{r} - r\right)\cos 2\phi + \left(\frac{1}{2}\left(r + \frac{1}{r}\right) - \cos\theta\right)\cos 4\phi \right) \tag{5.10}$$

Here, the parameters R and θ are scale-invariant. The scale dependence rises from the λ^{-4d} dependence of r, as well as the λ^{-4d} overall depenence. We may also note that the $\cos 2\phi$ term is antisymmetric under the xchange $r \rightarrow r^{-1}$. The other terms are symmetric under this exchange, hich corresponds to magnifying rather than reducing scales. We can oberve that, with the choice of $\cos\theta = 1$, the higher order terms vanish as $\rightarrow 1$, yielding ellipses at the appropriate scale. The choice of $\cos\theta = 0$ ields a system with the greatest degree of variation from the elliptical hape, as we see in section 5.4. The systems which are non-convex, i.e. hose whose $\cos 4\phi$ term is large in comparison to the angle-independent erm, are disallowed, as they result when $\cos\theta$ is negative.

Figure 2.1 shows the effect of having a large R^2 parameter; we see that ue to the dominance of the α_2 term for $a > 0$ (Eq. 3.7), for virtually all cales the contours are nearly straight. This effect is also to be noticed on elds with the same type of generator: except at the largest scales (corresponding to the small balls), the fields generated with this are extremely tratified (see Figure 4.1). Even when this is not the case, very 'streaky' elds are characteristic of the narrow rectangular small contours on 2.5 and .6 (corresponding to simulated fields 4.5 and 4.6).

Numbers 2.2–2.3 and 2.4–2.5 and the corresponding fields in Figure 5 how the effect of changing the initial value of r (i.e. $\lambda = 1$) on the shape of he balls, which is primarily one of increasing the apparent stratification of he field. The shape of the balls remains similar even with the changes in r nd in the GSI generator. The structures in the corresponding fields seem o be primarily affected in the mid-range of scales: the small scale microructures retain a similar appearance, as they correspond to the higherequency components of the balls in Fourier space, which are similar.

Additionally, Figures 2.7–2.8 and 4.7–4.8 together with 2.2 and 4.2 how the effect of changing θ. We note that, as we see in section 5.4, the ange of scales over which the system is "flattened" or "squirish" decreases s θ decreases.

5.3. Rotation dominant examples. Using the change of variables s in the second order case, we find that in r', ϕ coordinates the lines $r' =$ onstant are again ellipses. Taking the special case with $\alpha_1 = \beta_1 = 0$, we

eventually obtain the following for our balls:

$$r'(\phi)^{-4} = \lambda^{-4d}\frac{R^2}{2}(1 + R'\cos(4\phi - \zeta)) \tag{5.11}$$

where:

$$R'^2 = 1 - \left(\frac{2\sin\theta}{r + r^{-1}}\right)^2$$

$$R^2 = \alpha_{4,1}^2 + \alpha_{5,1}^2 + \beta_{4,1}^2 + \beta_{5,1}^2$$

and:

$$\tan\zeta = \frac{2\cos\theta}{r^{-1} - r}$$

where $r = |\underline{r}_5|/|\underline{r}_4|$ as before, and θ is the angle between $\underline{r}_5$ and $\underline{r}_4$. Thus this is an oscillation about an ellipse whose amplitude and phase depends on the ratio r, and angle θ. We note that as the scale ratio changes, R' is invariant, as is R; hence the basic anisotropy is fixed. Only the phase ζ changes, $\zeta \rightarrow \zeta - 4|a|u$, and the isotropic change of scale of r', given by the λ^{4d} term.

The anisotropy of this fourth order effect is determined by the ratio of the difference in the maximum and minimum r'^{-4} to the average R'; i.e the maximum anisotropy (the smaller the angle θ, the nearer $r(\lambda = 1)$ to 1), about the basic ellipse is obtained with parameters α, β which are directly limited by the crossing condition; the latter is a direct limitation of the amount of anisotropy possible about the basic ellipse. We find, however, in section 5.4, that the basic shape for rotation dominance is in fact (depending on R'), quite nonconvex, rather than elliptical.

Figure 3 shows the balls for varying unit ball parameters as well as for varying GSI generators, while Figure 5 shows the corresponding fields (simulated as above). The GSI parameters here are chosen to show slight rotation (Figs. 3.1–3.7) and a large degree of rotation dominance (Figs. 3.8, 3.9). Characterizing the curves as in Appendix A, we see that the maximum anisotropy about the ellipse is given for small θ and for $r(\lambda = 1)$ close to 1. This, as well as the observation that the basic anisotropy does not change for changing scale ratios, is confirmed by examining Figures 3.1 to 3.6. We note that all of these are nonconvex. In the rotation dominant case, however, the basic shape of the unit ball appears to depend more on the GSI generator than in the stratification dominant case, as may be noted by comparing Figure 3.8 to Figure 3.1. The differences in the balls are not as noticeable between 3.7 and 3.9; in this case, with $\theta = 1.5$ (that is, nearly $\pi/2$), and R' is near 0 (See Eq. 5.11), and the fields are convex (almost elliptical in appearance). Nonetheless, this difference is clearly noticeable in the simulated fields. The less strongly rotating field, Figure 5.7, is more

similar in texture to the other fields having the same generator, although the cross-hatching effect is less extreme than in the cases with the largest anisotropy. Figure 5.9 on the other hand is similar to Figure 5.8, and is more reminiscent of the ice field of Figure 1.2, with large bodies (floes) separated by the thinner fissure-like areas.

5.4. Characterization of the shapes. We now consider the morphology/shapes of the balls defined in the previous sections. Let us first discuss the interesting possibility of obtaining nonconvex closed fourth order curves. Consider the curve given by

$$I(\phi) = r'^{-4}(\phi) = (a + b\cos 2\phi + c\cos 4\phi) \tag{5.12}$$

where $a > 0$, $c > 0$, and a, b, c constrained so that $I > 0$. A convex ball will have a positive radius of curvature for all ϕ; a nonconvex ball will have a negative radius for at least some ϕ. The condition for convexity is:

$$I(4I + I'') - \frac{3}{16}I'^2 > 0 \tag{5.13}$$

Hence the direction of curvature changes only if this inequality is violated. Noting that $I > 0, I'^2 > 0$, it is obvious that a sufficient condition for nonconvexity is:

$$4I + I'' = a - 3c\cos 4\phi < 0 \tag{5.14}$$

i.e. $c > a/3$. Furthermore, when $b = 0$ (as in the rotation dominance case, eq. (5.11), the above condition is both necessary and sufficient and implies that if the scale-independent parameter $R' > \frac{1}{3}$, the balls are nonconvex; otherwise, they are convex. In the stratification dominant case the condition is that $\cos\theta < 0$: these crossing balls will be nonconvex. Further calculation shows conversely that all of the noncrossing cases ($\cos\theta > 0$) are convex. The case with $\cos\theta = 0$ corresponds to the existence of points of zero curvature at all scales (the curves also have points of osculation): nevertheless there is no change of sign of the curvature, and the balls are convex.

In these convex stratification dominant family of balls, there is nonetheless an interesting change in shape which occurs over a finite range of scales. Consider the extrema of the $r'(\phi)$ curves (as long as the Jacobian of the transformation of $DI/d\phi \rightarrow dr/d\theta$ - where r, θ are the usual polar coordinates - is non-zero it is sufficient to consider the number of zeroes of $dI/d\phi$). Here, the zeroes of I' are given by:

$$\sin 2\phi = 0,\ \cos 2\phi = -b/4c \tag{5.15}$$

Since for $0 \leq \phi < 2\pi$ the former equation always has four solutions. Elliptical balls will have two maxima and two minima. However, if $|b| < 4c$ then the system will have a total of 8 solutions, four maxima and four minima. This occurs when:

$$\cos\theta < r < \frac{1}{\cos\theta} \tag{5.16}$$

Thus, since r changes with scale change as λ^{-4a}, the system will pass through a set of scales at which it is flattened from the basic elliptical shape, becoming a "square ellipse" (see e.g. Fig. 2.5). The extreme cases of $\cos\theta = 0$ and $\cos\theta = 1$ are respectively flat and elliptical over the entire range of scales.

6. Conclusions. We have examined several subclasses of the particular family of fourth-order ball defined by Equations 5.1, 5.4 and 5.5, which when used together with the formalism of generalized scale invariance describe a number of interesting textures which may be relevant in various geophysical fields. One of the motivations for investigating this type of unit ball was to explain and examine the non-convex and other non-elliptical Fourier space contours noted in the case of ice fields, corresponding to the fissures and floes that characterize these physical fields. We have found that certain similar types of structure have been noticed in cases of rotation dominance, and that given the extension of these unit-ball families described in Section 5.1, parametrizations may be found for these structures in stratification dominant cases as well. These may not correspond exactly to the parameters in analyzing the ice data. Indeed, the work described here was in part motivated by the need to obtain empirical estimates of fourth order unit balls which would respect the non-crossing condition. There are some difficulties in analyzing the ice data for the shape of its unit ball (due in part to the large spread in the Fourier space contours of a real field; this is noise due to the fact that we analyze a single realization). Analysis procedures for these types of balls have been developed, but results as yet are inconclusive.

It has been demonstrated as well that the nature of the unit ball has great bearing on the morphology of the resulting field, in some cases apparently more so than the GSI generator; for example, it has been shown that given different parameters describing the unit ball, rotation dominant and stratification dominant fields can look similar over the finite range of scales we observe. Of course, it is impossible to choose the unit ball entirely independently of the GSI parameters: the generator of the field constrains the types of unit balls that are possible and still respect the non-crossing condition.

Within the restriction to fourth order balls, the question of course arises as to whether the examples that have been considered here are sufficiently general and inclusive, i.e. whether other useful qualitatively different fourth order polynomial balls exist. The full parameter space we are dealing with here is of course very large. In fact, an obvious step would be to increase the number of parameters by extending this to higher order polynomials;

the method outlined here readily lends itself to generalizations. However, this would seem to be unnecessary. The type of shapes expected from our fourth order polynomial parametrization of the unit ball are limited to fourth order oscillations about the second order (elliptical) shape. The sum of the pair of fourth order polynomials describing our unit ball thus allows (in the rotation dominant case) for nonconvex balls, square-like balls, and the somewhat elliptical balls (with or without some of the other types of effect). All these qualitative types of behaviour have been noted. Further increasing the order of the polynomial used to describe the unit ball would also seem to be unwarranted — the addition of higher order oscillations about the basic shape (limited by non-crossing conditions) would not seem to justify the increase in complexity. We expect that the families developed here will be useful complements to the elliptical families already available using quadratic balls; it is significant that both are obtained as special cases of the same quartic family described by eq. 5.1.

Further work, then, would entail developing more robust analysis techniques to determine the unit ball parameters of interesting fields with a greater degree of confidence. The basic method developed here could conceivably be extended to allow for nonlinear GSI; certainly, the application of non-crossing conditions to the unit balls and the resulting limitations on their shapes is necessary for nonlinear generators as well. Additionally, the idea of extending multiplicative cascades to vector and tensor quantities (i.e. Lie cascades [Schertzer and Lovejoy, 1995a]) rather than the scalar quantities currently assumed is an obvious and necessary one, given that the physics underlying these problems is vector and tensor in nature.

A. Appendix: Characterizing the curves.

Rotation dominant case: $a^2 < 0$:

A convenient characterization of the curves is given by the following change of variables:

$$\begin{aligned} r' \cos\phi &= cy - (e+f)x \\ r' \sin\phi &= |a|y \end{aligned} \tag{A.1}$$

The lines $r' =$ constant are ellipses with the following major and minor axes:

$$\frac{1}{\sqrt{(e+f)(e-\sqrt{c^2+f^2})}}, \quad \frac{1}{\sqrt{(e+f)(e+\sqrt{c^2+f^2})}} \tag{A.2}$$

with axes turned through an angle:

$$\tan^{-1}\left(\frac{c}{-f+\sqrt{c^2+f^2}}\right) \tag{A.3}$$

The anisotropy of the ellipses can be characterized by the difference in the squares of the axes divided by the sum of the squares:

$$\frac{\Delta(\text{squares})}{\sum(\text{squares})} = \frac{\sqrt{c^2+f^2}}{e} = \sqrt{1-\frac{|a|^2}{e^2}} \tag{A.4}$$

Since $a^2 < 0$, this ratio is bounded by 1, the larger it is, the more elongated the ellipses. For fixed e, anisotropy is a maximum for small $|a|$. In this new elliptical coordinate system, we have the following simplifications:

$$\begin{aligned} r'^2 &= \underline{x}^T \mathbf{m}_1 \underline{x} \\ r'^2 \cos 2\phi &= \underline{x}^T \mathbf{m}_4 \underline{x} \\ r'^2 \sin 2\phi &= \underline{x}^T \mathbf{m}_5 \underline{x} \end{aligned} \tag{A.5}$$

so that the basic second order polynomials take the simple form:

$$\underline{x}^T \mathbf{A}_1 \underline{x} = r'^2(\alpha_1 + \alpha_4 \cos 2\phi + \alpha_5 \sin 2\phi) \tag{A.6}$$

Taking the case $\alpha_1 = 0$, the curve $f_\lambda(\underline{x}) = 1$ now becomes:

$$r'(\phi)^{-4} = \frac{|\underline{\alpha}|^2 + |\underline{\beta}|^2}{2}(1 + R' \cos(4\phi - \zeta)) \tag{A.7}$$

$$\lambda^{-4d}\frac{R^2}{2}(1 + R' \cos(4\phi - \zeta))$$

where

$$R'^2 = 1 - \left(\frac{2\sin\theta}{r + r^{-1}}\right)^2$$

$$R^2 = \alpha_{4,1}^2 + \alpha_{4,1}^2 + \alpha_{5,1}^2 + \beta_{4,1}^2 + \beta_{5,1}^2$$

and;

$$\tan\zeta = \frac{2\cos\theta}{r^{-1} - r}$$

where $r = |\underline{r}_s|/|\underline{r}_4|$ as before, and θ is the angle between $\underline{r}_5$ and $\underline{r}_4$.

Stratification dominance case: $a^2 \geq 0$:

We start with an analogous change of variables in this case:

$$\begin{aligned} r' \cos\phi &= \frac{1}{\sqrt{2}}(-(e+f)x + (c-a)y) \\ r' \sin\phi &= \frac{1}{\sqrt{2}}(-(e+f)x + (c+a)y) \end{aligned} \tag{A.8}$$

The curves $r' =$ constant are ellipses similar to those above. The rresponding eigenvalues whose reciprocal root gives the major and minor es are:

(A.9) $c^2+ef+f^2+\sqrt{c^2a^2+e^2(e+f^2)}; c^2+ef+f^2-\sqrt{c^2a^2+e^2(e+f^2)}$

he corresponding angle is given by

(A.10) $$\tan^{-1}\left(\frac{c(e+f)}{-c^2+ef+f^2+\sqrt{c^2a^2+e^2(e+f^2)}}\right)$$

Similarly:

(A.11) $$\begin{aligned} r'^2\sin 2\phi &= \underline{x}^T\mathbf{m}_1\underline{x} \\ r'^2(1-\cos 2\phi) &= \underline{x}^T\mathbf{m}_2\underline{x} \\ r'^2(1+\cos 2\phi) &= \underline{x}^T\mathbf{m}_3\underline{x} \end{aligned}$$

and

(A.12) $$\underline{x}^T\mathbf{A}_1\underline{x} = r'^2(\alpha_2+\alpha_3+(\alpha_2-\alpha_3)\cos 2\phi+\alpha_1\sin 2\phi)\ .$$

We now obtain:

(A.13) $$\begin{aligned} r'^{-4}(\phi) &= (\alpha_2^2+\beta_2^2)\left(\frac{3}{2}(r^2+1)+r\cos\theta+2(1-r^2)\cos 2\phi\right. \\ &\qquad \left.+\left(\frac{1}{2}(r^2+1)-r\cos\theta\right)\cos 4\phi\right) \\ &= \lambda^{-4d}R\left(\frac{3}{2}\left(r+\frac{1}{r}\right)+\cos\theta+2\left(\frac{1}{r}-r\right)\cos 2\phi\right. \\ &\qquad \left.+\left(\frac{1}{2}\left(r\frac{1}{r}\right)-\cos\theta\right)\cos 4\phi\right) \end{aligned}$$

with

$$R^2 = \sqrt{(\alpha_{2,1}^2+\beta_{2,1}^2)(\alpha_{3,1}^2+\beta_{3,1}^2)}$$

where $r = |\underline{r}_3|/|\underline{r}_2|$ and θ is the angle between $\underline{r}_3$ and $\underline{r}_2$. R and θ are invariant under scale transformations; r is given by

(A.14) $$r = \lambda^{-4a}\sqrt{\frac{(\alpha_3^2+\beta_3^2)}{(\alpha_2^2+\beta_2^2)}}$$

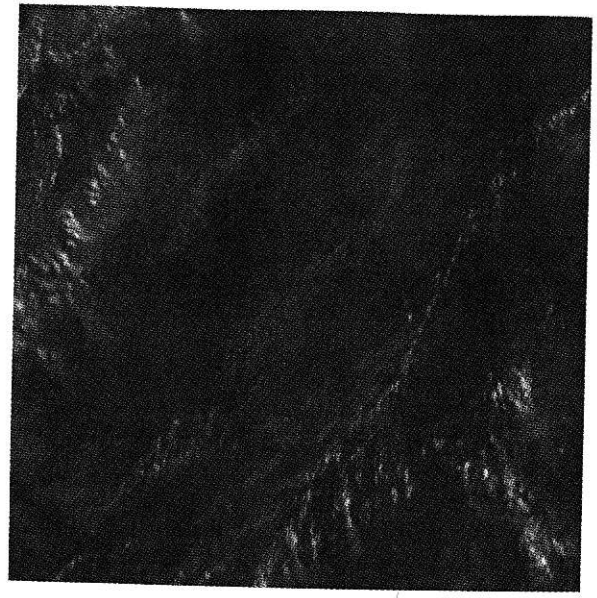

Figure 1.1a) NOAA-9 cloud image, visible spectrum (channel 1)

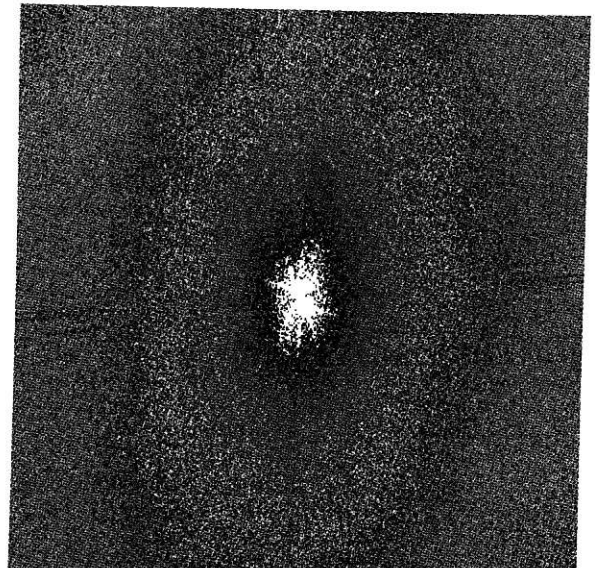

Figure 1.1b) 2-D power spectrum of image a)

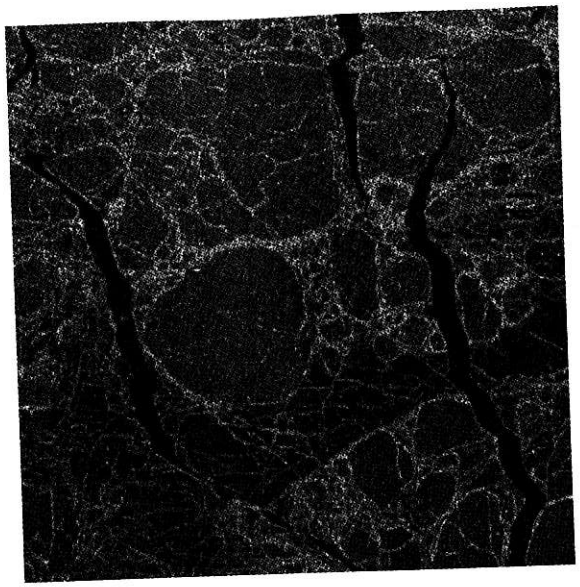

Figure 1.2a) SAR sea ice image

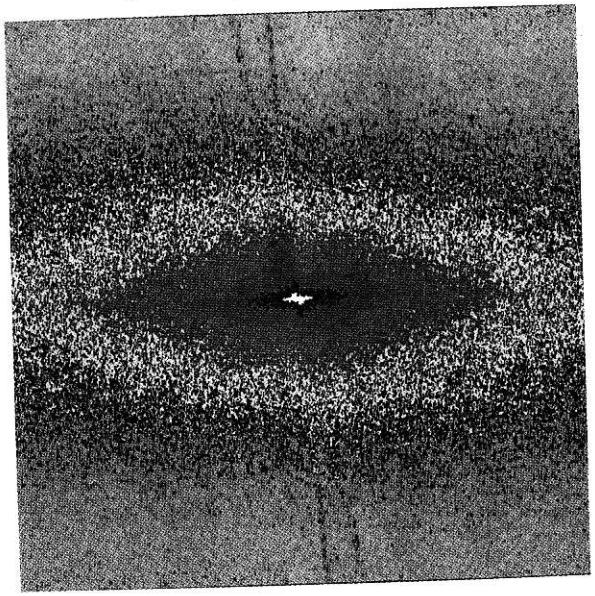

Figure 1.2b) 2-D power spectrum of image a)

Figure 2: Examples of stratification dominant balls

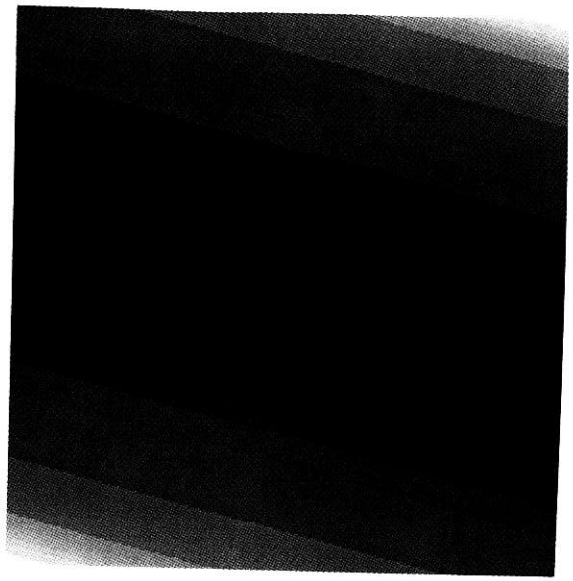

Figure 2.1: c=0.4, f=0.1, e=0.1; r=1.0, $\theta = 0.5, R^2 = 1.0$

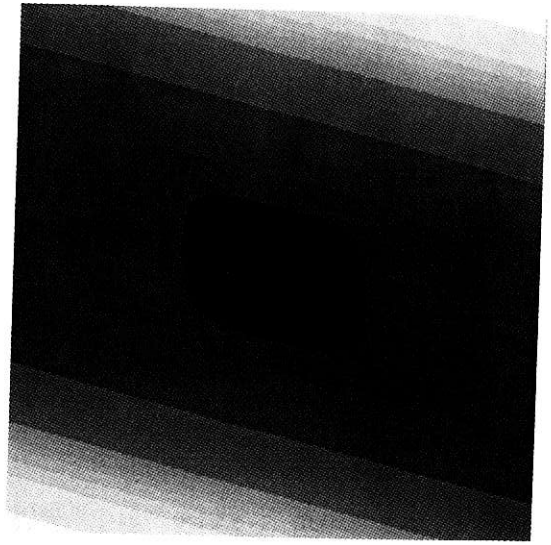

Figure 2.2: c=0.4, f=0.1, e=0.1; r=5.0, $\theta = 1.5, R^2 = 1.0 \times 10^{-6}$

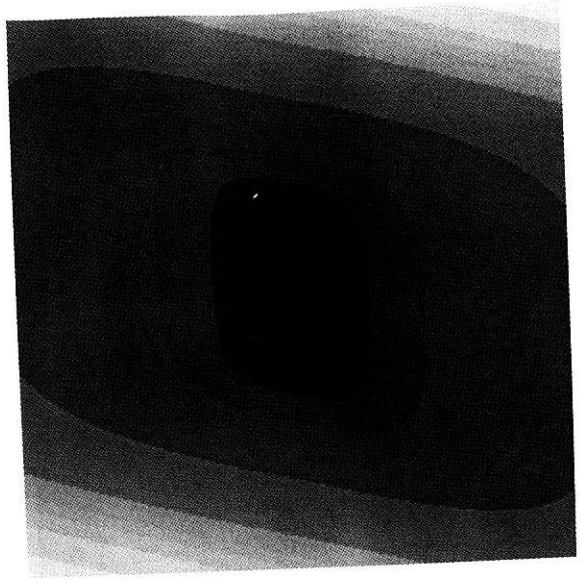

Figure 2.3: c=0.4, f=0.1, e=0.1; r=50.0, $\theta = 1.5, R^2 = 1.0 \times 10^{-6}$

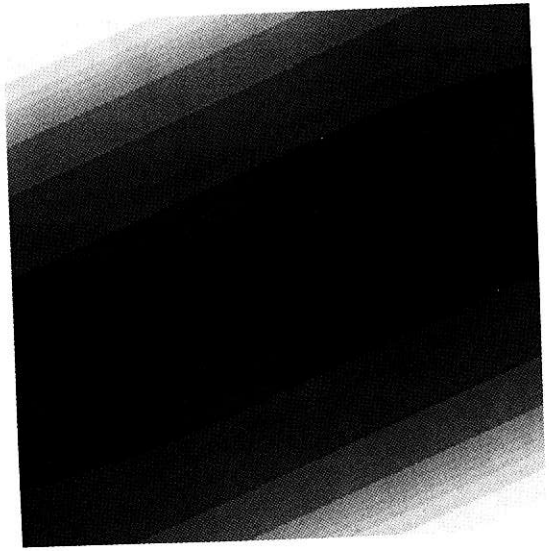

Figure 2.4: c=0.1, f=-0.8, e=0.5; r=1.0, $\theta = 1.5, R^2 = 1.0 \times 10^{-6}$

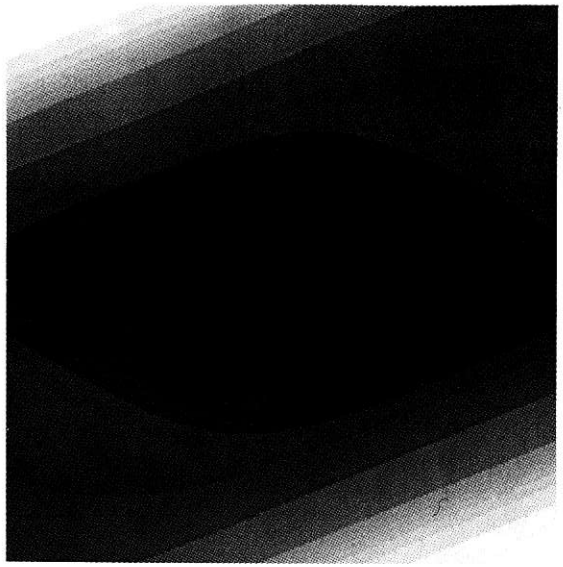

Figure 2.5: c=0.1, f=-0.8, e=0.5; r=50.0, $\theta = 1.5, R^2 = 1.0 \times 10^{-6}$

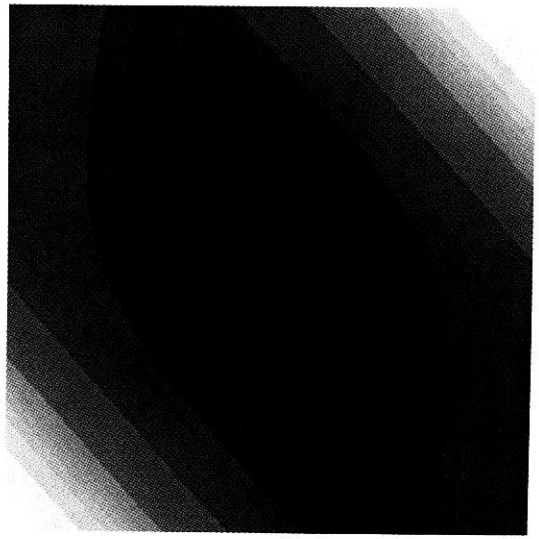

Figure 2.6: c=0.5, f=0.7, e=0.57; r=5.0, $\theta = 0.2, R^2 = 1.0 \times 10^{-6}$

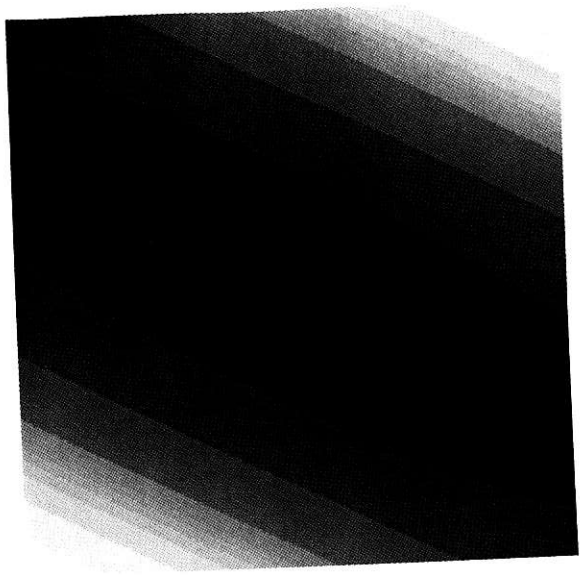

Figure 2.7: c=0.4, f=0.1, e=0.1; r=1.0, $\theta = 1.0, R^2 = 1.0 \times 10^{-6}$

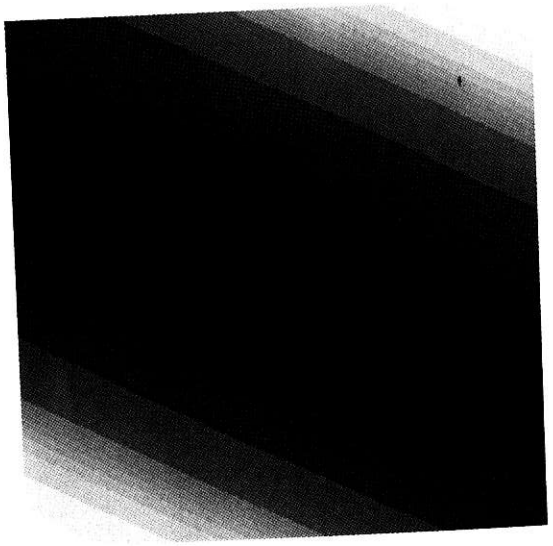

Figure 2.8: c=0.4, f=0.1, e=0.1; r=1.0, $\theta = 0.5, R^2 = 1.0 \times 10^{-6}$

Figures 3: Examples of rotation dominant balls

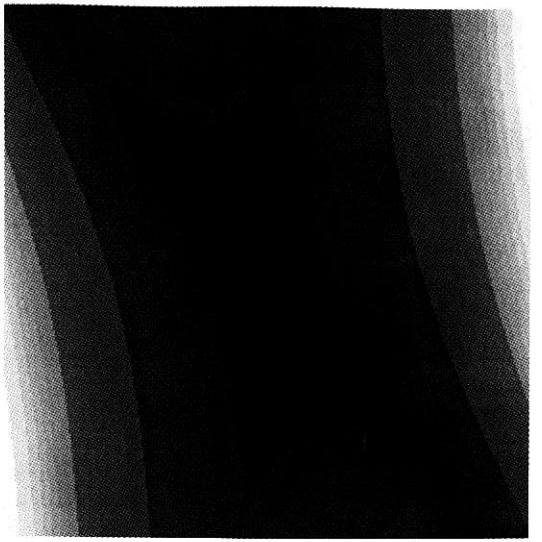

Figure 3.1: c=0.1, f=0.1, e=0.2; r=1.0, $\theta = 0.5, R^2 = 1.0$

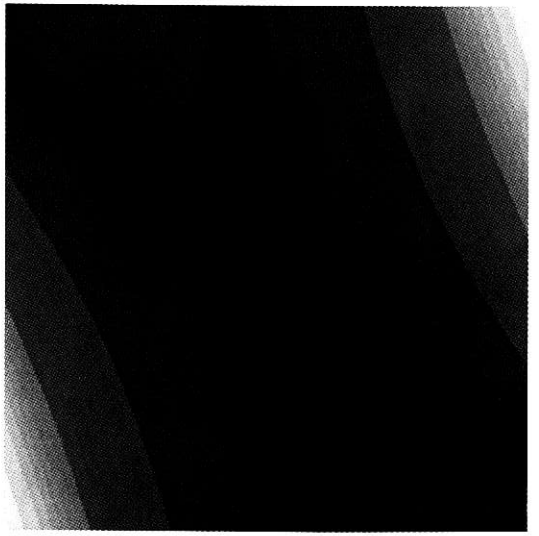

Figure 3.2: c=0.1, f=0.1, e=0.2; r=5.0, $\theta = 0.5, R^2 = 1.0$

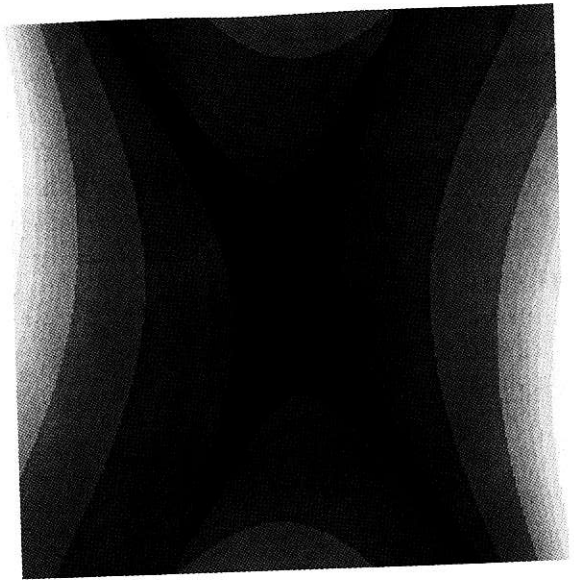

Figure 3.3: c=0.1, f=0.1, e=0.2; r=0.1, $\theta = 0.5, R^2 = 1.0$

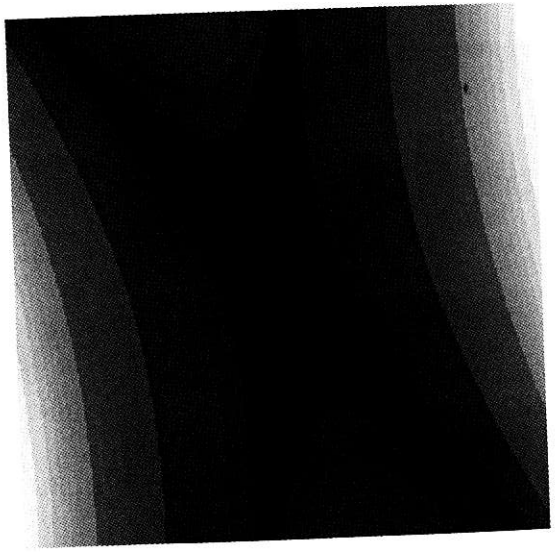

Figure 3.4 c=0.1, f=0.1, e=0.2; r=1.0, $\theta = 0.2, R^2 = 1.0$

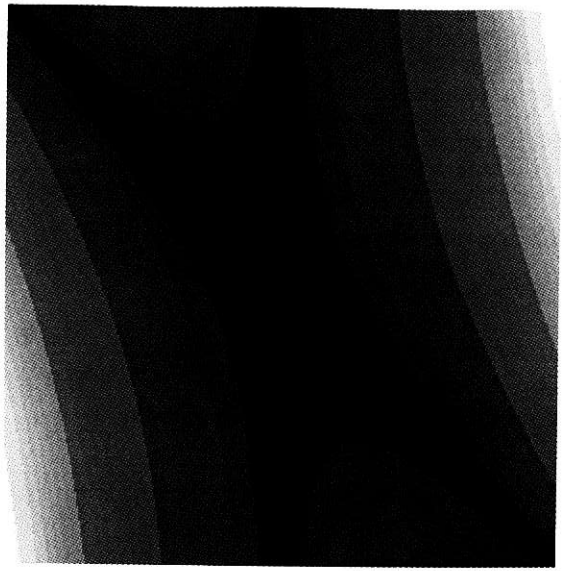

Figure 3.5: c=0.1, f=0.1, e=0.2; r=1.0, $\theta = 0.2, R^2 = 0.05$

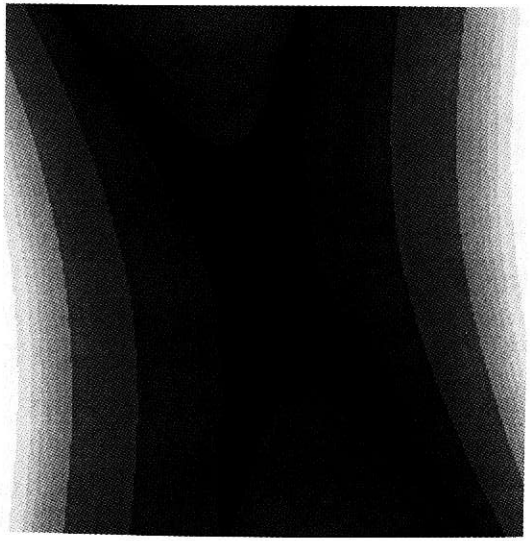

Figure 3.6: c=0.1, f=0.1, e=0.2; r=1.0, $\theta = 0.2, R^2 = 20.0$

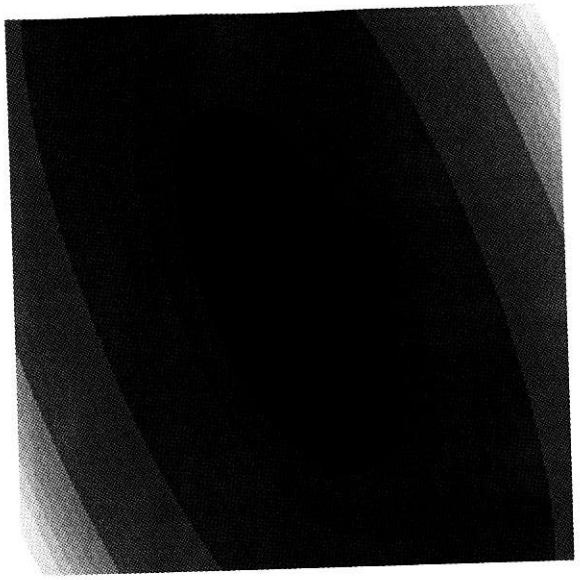

Figure 3.7: c=0.1, f=0.1, e=0.2; r=1.0, $\theta = 1.5, R^2 = 1.0$

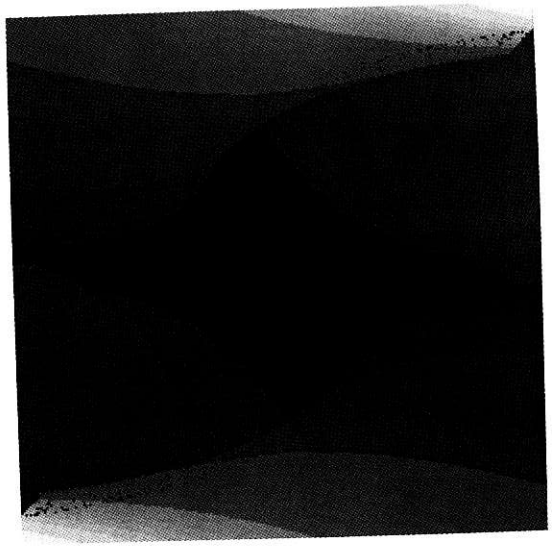

Figure 3.8: c=0.2, f=-0.5, e=1.0; r=1.0, $\theta = 0.5, R^2 = 1.0$

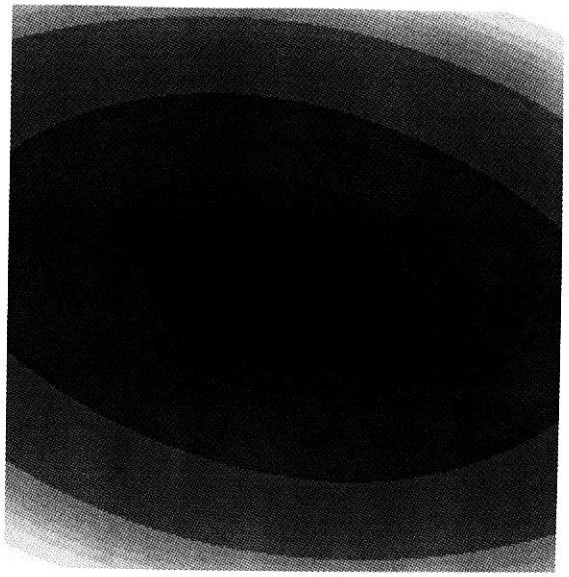

Figure 3.9: c=0.2, f=-0.5, e=1.0; r=1.0, $\theta = 1.5, R^2 = 0.05$

Figure 4: Real-space simulated fields corresponding to Fig. 2

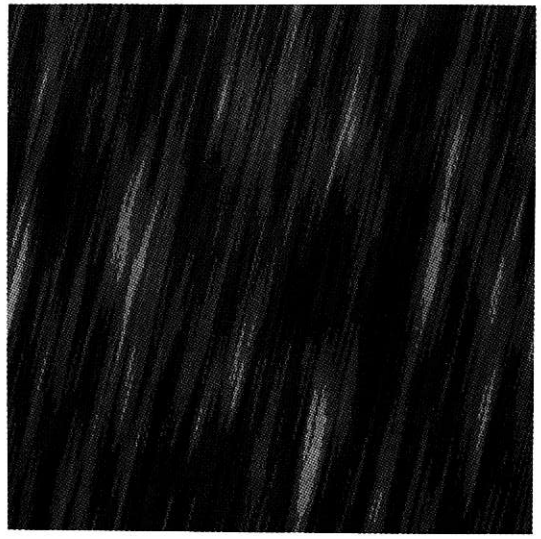

Figure 4.1: c=0.4, f=0.1, e=0.1; r=1.0, $\theta = 0.5, R^2 = 1.0$

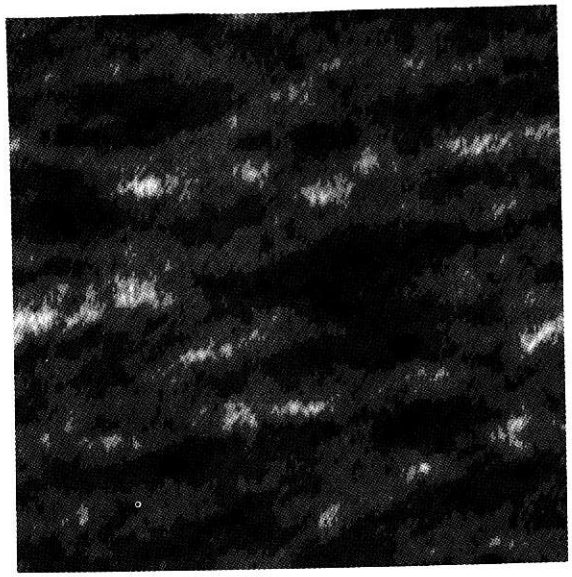

Figure 4.2: c=0.4, f=0.1, e=0.1; r=5.0, $\theta = 1.5, R^2 = 1.0 \times 10^{-6}$

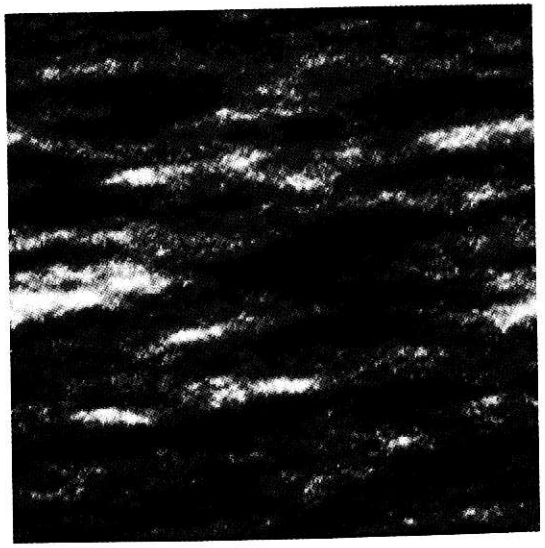

Figure 4.3: c=0.4, f=0.1, e=0.1; r=50.0, $\theta = 1.5, R^2 = 1.0 \times 10^{-6}$

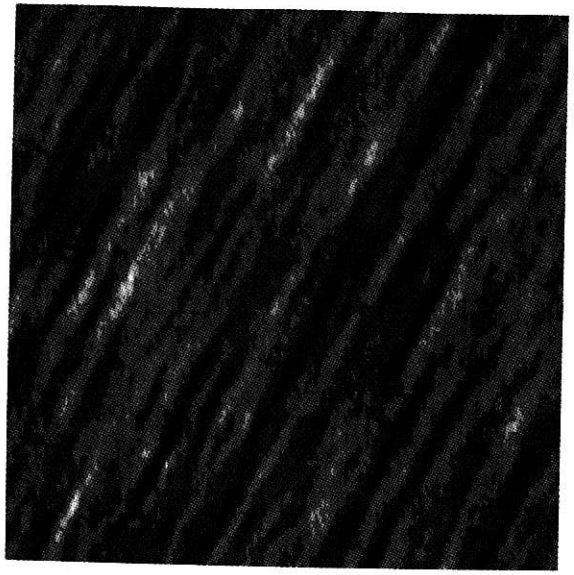

Figure 4.4: c=0.1, f=-0.8, e=0.5; r=1.0, $\theta = 1.5, R^2 = 1.0 \times 10^{-6}$

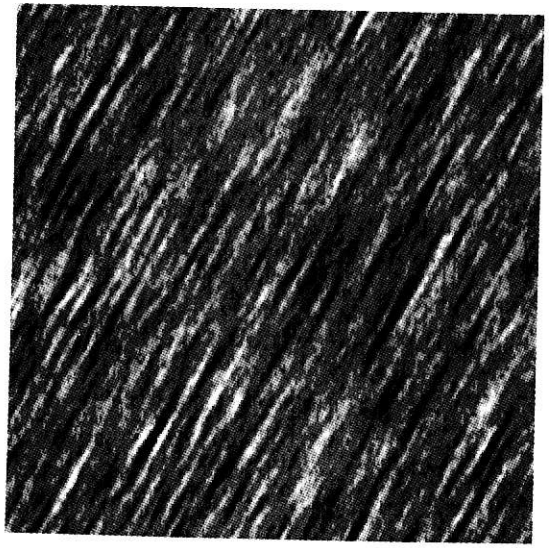

Figure 4.5: c=0.1, f=-0.8, e=0.5; r=50.0, $\theta = 1.5, R^2 = 1.0 \times 10^{-6}$

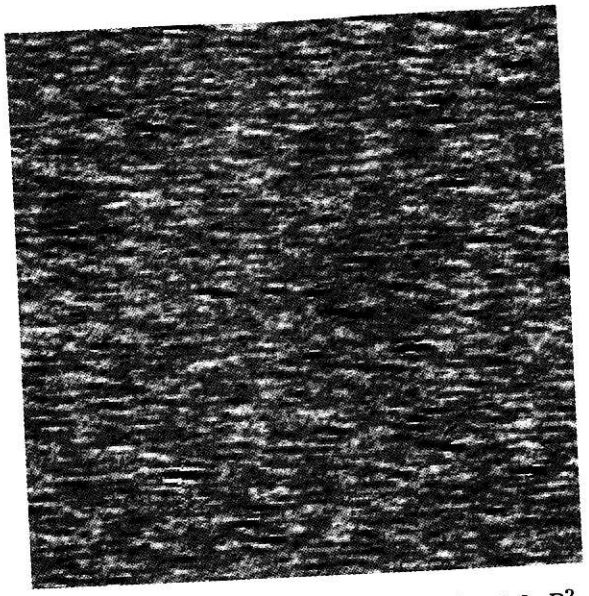

Figure 4.6: c=0.5, f=0.7, e=0.57; r=5.0, $\theta = 0.2, R^2 = 1.0 \times 10^{-6}$

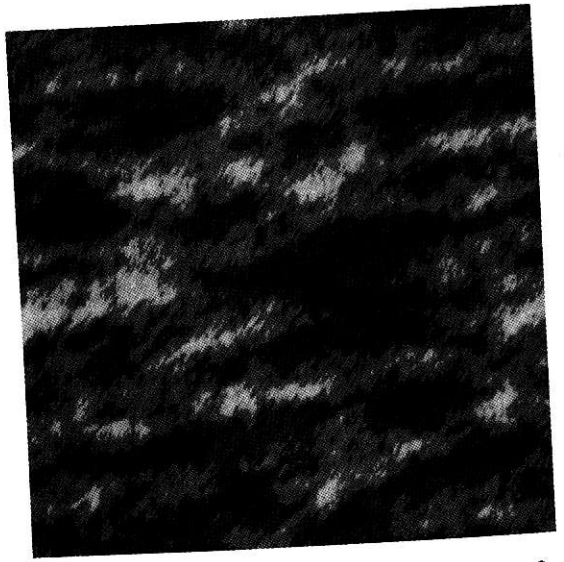

Figure 4.7: c=0.4, f=0.1, e=0.1; r=1.0, $\theta = 1.0, R^2 = 1.0 \times 10^{-6}$

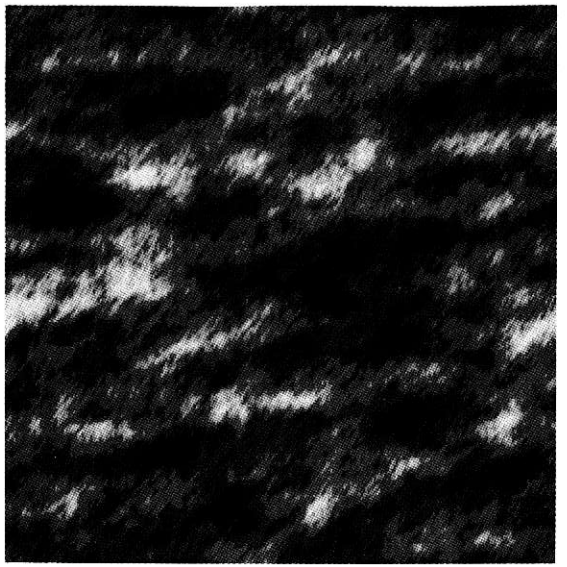

Figure 4.8: c=0.4, f=0.1, e=0.1; r=1.0, $\theta = 0.5, R^2 = 1.0 \times 10^{-6}$

Figure 5: Real-space simulated fields corresponding to Fig. 3

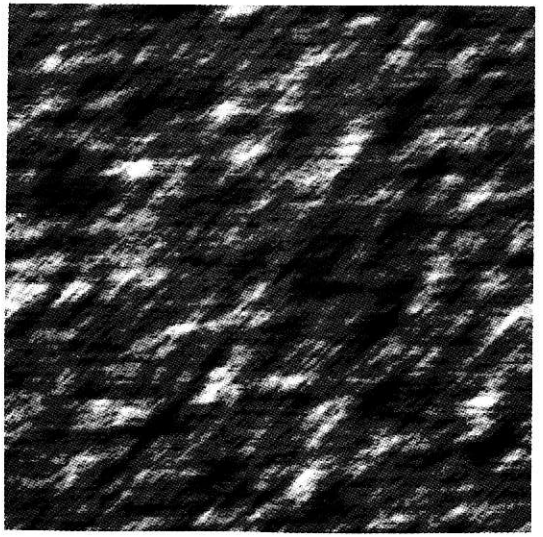

Figure 5.1: c=0.1, f=0.1, e=0.2; r=1.0, $\theta = 0.5, R^2 = 1.0$

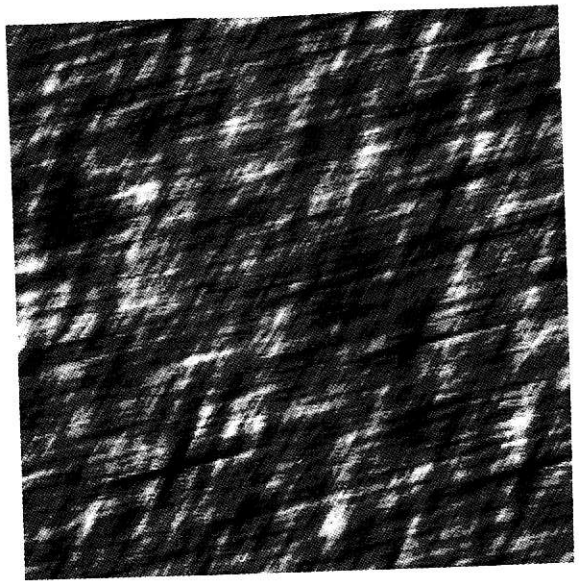

Figure 5.2: c=0.1, f=0.1, e=0.2; r=5.0, $\theta = 0.5, R^2 = 1.0$

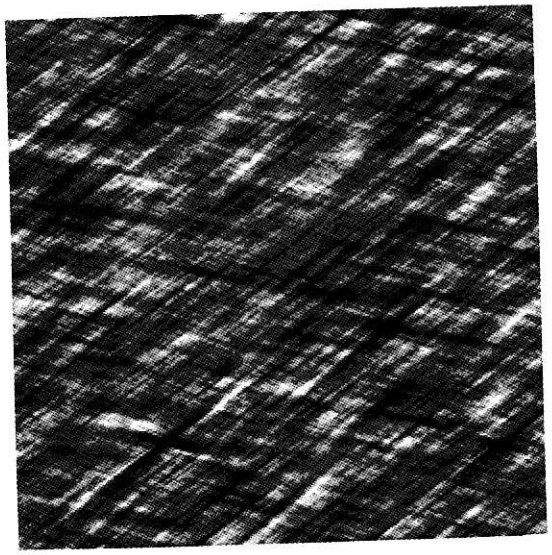

Figure 5.3: c=0.1, f=0.1, e=0.2; r=0.1, $\theta = 0.5, R^2 = 1.0$

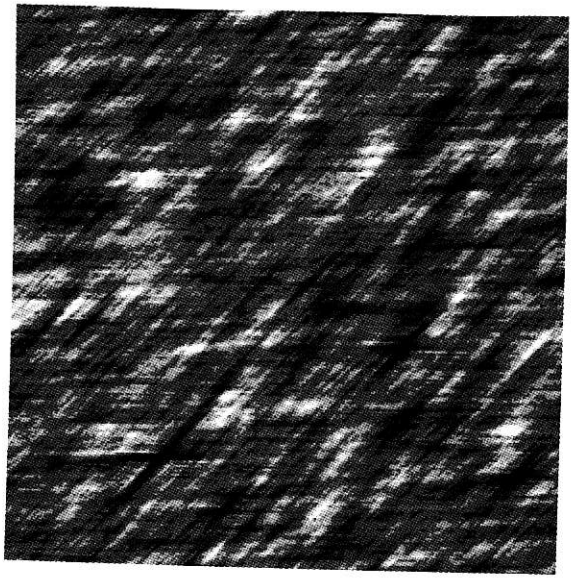

Figure 5.4: c=0.1, f=0.1, e=0.2; r=1.0, $\theta = 0.2, R^2 = 1.0$

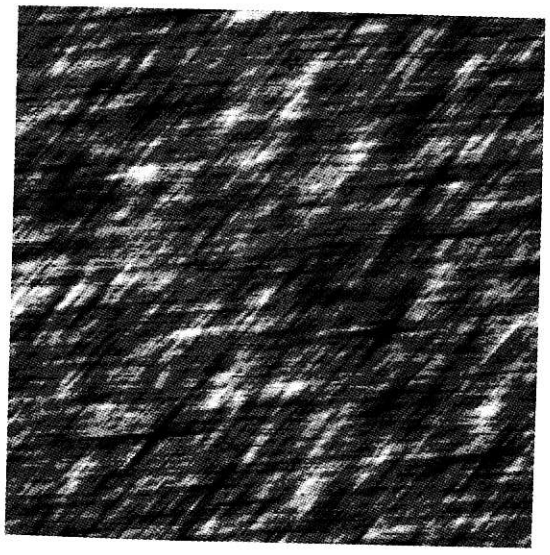

Figure 5.5: c=0.1, f=0.1, e=0.2; r=1.0, $\theta = 0.2, R^2 = 0.05$

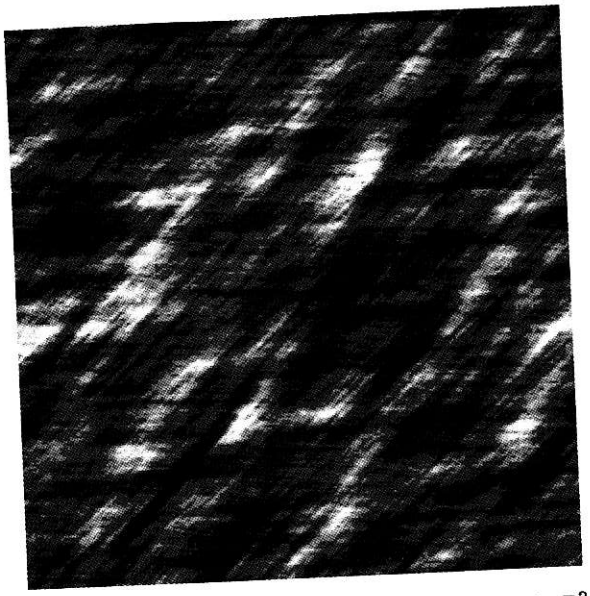

Figure 5.6: c=0.1, f=0.1, e=0.2; r=1.0, $\theta = 0.2, R^2 = 20.0$

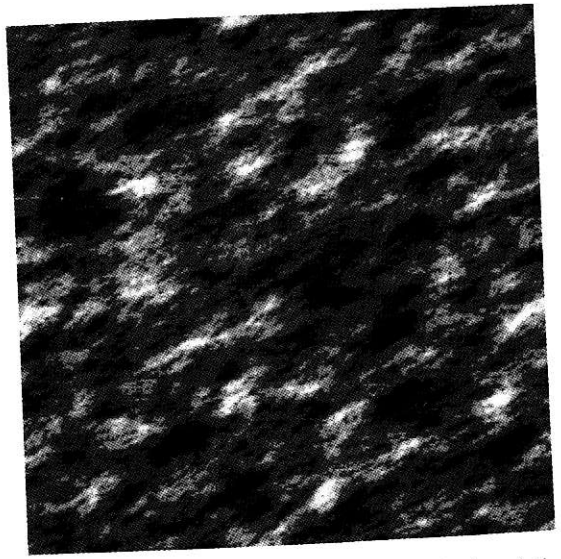

Figure 5.7: c=0.1, f=0.1, e=0.2; r=1.0, $\theta = 1.5, R^2 = 1.0$

Figure 5.8: c=0.2, f=-0.5, e=1.0; r=1.0, $\theta = 0.5, R^2 = 1.0$

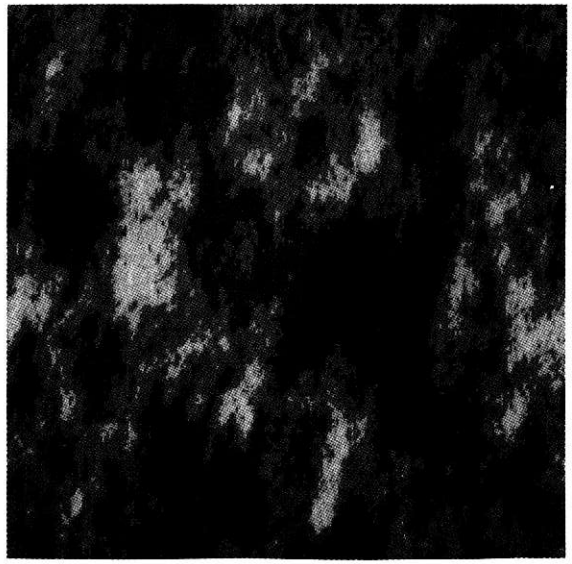

Figure 5.9: c=0.2, f=-0.5, e=1.0; r=1.0, $\theta = 1.5, R^2 = 0.05$

REFERENCES

Chigirinskaya, Y., D. Schertzer, S. Lovejoy, A. Lazarev, and A. Ordanovich, *Unified multifractal atmospheric dynamics tested in the tropics Part 1: horizontal scaling and self-organized criticality*, Nonlinear Processes in Geophysics (1), 105–114, 1994.

Davis, A., S. Lovejoy, and D. Schertzer, *Supercomputer simulation of radiative transfer inside multifractal cloud models*, in I.R.S. 92, edited by S. Keevallik and O. Kärner, 112–115, 1992.

Falco, T., F. Francis, S. Lovejoy, D. Schertzer, B. Kerman, and M. Drinkwater, in *IEEE Transactions on Geosciences and Remote Sensing*, 34, 906–914, 1996.

Fox, C.G., and D. Hayes, *Quantitative methods for analyzing the roughness of the seafloor*, Reviews of Geophysics (23), 1–48, 1985.

Frisch, U.P., P.L. Sulem, and M. Nelkin, *A Simple Dynamical Model of Intermittency in Fully Developed Turbulence*, Journal of Fluid Mechanics, 87, 719–24, 1978.

Gabriel, P., S. Lovejoy, D. Schertzer, and G.L. Austin, *Multifractal Analysis of resolution dependence in satellite imagery*, Journal of Geophysical Research, 15, 1373–1376, 1988.

Gupta, V.K., and E. Waymire, *A Statistical Analysis of Mesoscale Rainfall as a Random Cascade*, Journal of Applied Meteorology, 32, 251–267, 1993.

Hooge, C., *Earthquakes as a Space-Time multifractal Process*, M. Sc. thesis, McGill University, Montreal (Qeubec), Canada, 1993.

Hooge, C., S. Lovejoy, D. Schertzer, S. Pecknold, J.-F. Malouin, and F. Schmitt, *Multifractal Phase Transitions: The Origin of Self-Organized Criticality in Earthquakes*, Non-Linear Processes in Geophysics, 1 (2), 191–197, 1994.

Lavallée, D., S. Lovejoy, D. Schertzer, and P. Ladoy, *Nonlinear variability and landscape topography: analysis and simulation*, in *Fractals in geography*, edited by L. De Cola, and N. Lam, pp. 171–205, Prentice-Hall, 1993.

Lazarev, A., D. Schertzer, S. Lovejoy, and Y. Chigirinskaya, *Unified multifractal atmospheric dynamics tested in the tropics Part II: vertical scaling and generalized scale invariance*, *Nonlinear Processes in Geophysics* (1), 115–123, 1994.

Lewis, G., S. Lovejoy, and D. Schertzer, *The scale invariant générator technique for parameter estimates in generalized scale invariant systems*, Computers in Geoscience (submitted), 1996.

Lovejoy, S., D. Lavallée, D. Schertzer, and P. Ladoy *The $\ell^{1/2}$ law and multifractal topography: theory and analysis*, *Nonlinear Processes in Geophysics* (2), 16–22, 1995.

Lovejoy, S., and D. Schertzer, *Generalized Scale Invariance in the Atmosphere and Fractal Models of Rain*, Water Resources Research, 21 (8), 1233–1250, 1985.

Lovejoy, S., and D. Schertzer, *Our multifractal atmosphere: A unique laboratory for non-linear dynamics*, Physics in Canada, 46, 62, 1990.

Lovejoy, S., and D. Schertzer, *How bright is the coast of Brittany?*, in *Fractals in Geoscience and Remote Sensing*, edited by G. Wilkinson, I. Kanellopoulos, and J. Mgier,. 102–151, Office for Official Publications of the European Communities, Luxembourg, 1995.

Lovejoy, S., D. Schertzer, and K. Pflug, *Generalized Scale Invariance and differentially rotation in cloud radiances*, Physica A, 185, 121–127, 1992.

Lovejoy, S., D. Schertzer, and A.A. Tsonis, *Functional Box-Counting and Multiple Dimensions in rain*, Science, 235, 1036–1038, 1987.

Mandelbrot, B.B., *Intermittent turbulence in self-similar cascades: divergence of high moments and dimension of the carrier*, Journal of Fluid Mechanics, 62, 331–350, 1974.

Meneveau, C., K.R. Sreenivasan, P. Kailasnah, and M.S. Fan, *Joint multifractal measures: theory and applications to turbulence*, Physical Review A, 41, 894, 1990.

Novikov, E.A., and R. Stewart, *Intermittency of turbulence and spectrum of fluctuations in energy-dissipation*, Izv. Akad. Nauk. SSSR. Ser. Geofiz., 3, 408–412, 1964.

Pecknold, S., S. Lovejoy, D. Schertzer, C. Hooge, and J.-F. Malouin, *The Simulation of Universal Multifractals*, in *Cellular Automata: Prospects in Astrophysical Applications*, edited by A. Lejeune, and J. Perdang, pp. 228–67, World Scientific, Singapore, 1993.

Pflug, K., S. Lovejoy, and D. Schertzer, *Generalized Scale Invariance, differential rotation and cloud texture*, in *Nonlinear dynamics of Structures*, edited by R.Z. Sagdeev, U. Frisch, A.S. Moiseev, and A. Erokhin, 72–78, World Scientific, 1991.

Pflug, K., S. Lovejoy, and D. Schertzer, *Differential Rotation and Cloud Texture: Analysis Using Generalized Scale Invariance*, Master's of Science Thesis thesis, McGill University, 1992.

Pflug, K., S. Lovejoy, and D. Schertzer, *Generalized Scale Invariance, differential rotation and cloud texture*, Journal of Atmospheric Sciences, 50, 538–553, 1993.

Pilkington, M., and J.P. Todoeschuk, *Fractal Magnetization of Continental Crust*, *Geophysical Research Letter*, 20 (7), 627–630, 1993.

Schertzer, D., and S. Lovejoy, *On the Dimension of Atmospheric motions*, in *Turbulence and Chaotic phenomena in Fluids*, IUTAM, edited by T. Tatsumi, 505–512, Elsevier Science Publishers B. V., 1984.

Schertzer, D., and S. Lovejoy, *The dimension and intermittency of atmospheric dynamics*, in *Turbulent Shear Flows 4*, edited by B. Launder, 7–33, Springer, 1985a.

Schertzer, D., and S. Lovejoy, *Generalised scale invariance in turbulent phenomena*, Physico-Chemical Hydrodynamics Journal, 6, 623–635, 1985b.

Schertzer, D., and S. Lovejoy, *Physical modeling and Analysis of Rain and Clouds by Anysotropic Scaling of Multiplicative Processes*, Journal of Geophysical Research, D 8 (8), 9693–9714, 1987.

Schertzer, D., and S. Lovejoy, *Generalized Scale Invariance and multiplicative processes in the atmosphere*, PAGEOPH, 130, 57–81, 1989.

Schertzer, D., and S. Lovejoy, *Nonlinear geodynamical variability: multiple singularities, universality and observables*, in *Non-linear variability in geophysics: Scaling and Fractals*, edited by D. Schertzer, and S. Lovejoy, 41–82, Kluwer, 1991a.

Schertzer, D., and S. Lovejoy, *Scaling Nonlinear Variability in Geodynamics*, in *Nonlinear Variability in Geophysics: Scaling and Fractals*, edited by D. Schertzer, and S. Lovejoy, 41–82, Kluwer Academic Publishers, Dordrecht, 1991b.

Schertzer, D., and S. Lovejoy, *From scalar cascades to Lie cascades: joint multifractal analysis of rain and cloud processes*, in *Space/time Variability and Interdependance for various hydrological processes*, edited by R.A. Feddes, 153–173, Cambridge University Press, New-York, 1995a.

Schertzer, D., and S. Lovejoy, *The multifractal phase transition route to self-organized criticality*, Physics Reports, in press, 1996.

Schmitt, F., D. Lavallée, D. Schertzer, and S. Lovejoy *Empirical Determination of Universal Multifractal Exponents in Turbulent Velocity Fields*, Physical Review Letter, 68, 305–308, 1992.

Schmitt, F., D. Schertzer, and S. Lovejoy, and Y. Brunet, *Estimation of universal multifractal indices for atmospheric turbulent velocity fields*, Fractals, 3, 568–575.

Tessier, Y., S. Lovejoy, and D. Schertzer, *Universal Multifractals: theory and observations for rain and clouds*, Journal of Applied Meteorology, 32 (2), 223–250, 1993a.

Tessier, Y., S. Lovejoy, D. Schertzer, D. Lavallée, and B. Kerman, *Universal Multifractal Indices For The Ocean Surface At Far Red Wavelengths*, Geophysical Research Letter, 20 (12), 1167–1170, 1993b.

Van Zandt, T.E., S.A. Smith, T. Tsuda, D.C. Fritts, T. Sato, S. Fukao, and S. Kato, *Studies of Velocity Fluctuations in the Lower Atmosphere Using the MU Radar*, Part I: Azimuthal Anisotropy, J. Atmos. Sci. (47), 39–50, 1990.

Veneziano, D., G. Moglen, and R.L. Bras, *Iterate random pulse processes and their spectral properties*, Water Resources (submitted), 1996.

Yaglom, A.M., *The influence on the fluctuation in energy dissipation on the shape of turbulent characteristics in the inertial interval*, Sov. Phys. Dokl., 2, 26–30, 1966.